Published in Combustion and Flame
https://doi.org/10.1016/j.combustflame.2017.03.030

Comparative experimental and modeling study of the low- to moderate-temperature oxidation chemistry of 2,5-dimethylfuran, 2-methylfuran, and furan

Luc-Sy Tran[1,*], Zhandong Wang[1,#], Hans-Heinrich Carstensen[2], Christian Hemken[1], Frédérique Battin-Leclerc[3], Katharina Kohse-Höinghaus[1,*]

[1] *Department of Chemistry, Bielefeld University, Universitätsstraße 25, D-33615 Bielefeld, Germany*

[2] *Laboratory for Chemical Technology (LCT), Ghent University, Technologiepark 914, 9052 Ghent, Belgium*

[3] *Laboratoire Réactions et Génie des Procédés, UMR 7274 CNRS - Université de Lorraine, 1 rue Grandville, 54000 Nancy, France*

[#] *Current address: Clean Combustion Research Center, King Abdullah University of Science and Technology, Thuwal 23955-6900, Saudi Arabia*

* Corresponding authors:
Luc-Sy Tran: luc-sy.tran@uni-bielefeld.de
Katharina Kohse-Höinghaus: kkh@uni-bielefeld.de

Color figures in electronic version only

Supplemental Material is available

Abstract

The reaction chemistry of furanic fuels, proposed as next-generation bio-derived fuels, has been a target of recent studies. However, quantitative intermediate species profiles at low- to moderate-temperature (LMT) conditions remain scarce. The present paper reports the first systematic full speciation dataset in the temperature range 730-1170 K for three furanic fuels, 2,5-dimethylfuran (DMF), 2-methylfuran (MF), and furan, measured for different equivalence ratios under near-identical LMT conditions in a flow reactor at 1 bar. More than 35 species including reactants, intermediate species, and products were analyzed using electron ionization (EI) molecular-beam mass spectrometry (MBMS). These experimental results provided motivation to extend a previous single joint mechanism for the three furanic fuels, developed for the high-temperature regime in low-pressure premixed flames, to include the LMT oxidation chemistry. A decisive difference of the present mechanism versus all previously reported models is a more complete description of fuel radical reactions for LMT oxidation, obtained from theoretical calculations of thermodynamic properties and rate constants.

The experimentally observed differences in fuel conversion behavior and species distribution between the three fuels have been compared to model predictions using the newly extended mechanism. The dependence of fuel conversion on equivalence ratio decreases significantly from DMF to furan, a behavior consistent with the different number of lateral methyl groups in the fuel structure. All three furanic fuels, especially DMF, produce several highly toxic oxygenated species including acrolein, methyl vinyl ketone, furfural, and phenol. These toxic species were found to be products of the primary reactions of these fuels, and these undesirable trends could be explained satisfactorily by the present model, pointing to some caution with regard to the potential emission spectra under LMT conditions.

Keywords: Furan, 2-methylfuran, 2,5-dimethylfuran, flow reactor, low- to moderate-temperature oxidation, detailed kinetic model.

1. Introduction

Saturated and unsaturated cyclic ethers such as the derivatives of tetrahydrofuran (THF) and furan, respectively, are being proposed as alternative fuels [1-6]. They are potentially accessible from cellulosic biomass [7-9]. Their properties, including high octane numbers, make them desirable for spark-ignition applications [2-4,6]. Also, these fuels have recently been used as additives for diesel engines [1,5,10,11]. 2-Methyl-THF in blending with *n*-dibutylether (70%/30% by volume) was found to almost entirely reduce particle emissions from a diesel engine [1]. Furan derivatives showed a superior soot reduction potential compared to *n*-butanol, *n*-heptane, cetanes, and gasoline in blends with diesel fuel [5,10,11]. Because of the presence of double bonds, unsaturated cyclic ethers exhibit a very different oxidation behavior from saturated cyclic ethers [6,12-14]. Furthermore, while some THF derivatives show a negative-temperature-coefficient (NTC) behavior, the latter has not be observed for furans [14-17]. The present paper focusses on the oxidation chemistry of the three *unsaturated cyclic ethers* of the furan family, *e.g.* 2,5-dimethylfuran (DMF), 2-methylfuran (MF), and furan, here called "furanic". Therefore, the following discussions will address only these fuels.

Considerable interest has been devoted to the high-temperature (HT) oxidation chemistry of furanic fuels, *e.g.*, reporting premixed flame speciation [18-23], shock tube ignition [17,24-27], and flame speed [17,27] experiments as well as model developments [17-19,24,28]. Xu *et al*. [29] have recently presented an overview of such studies. Only limited work has addressed, however, the low- to moderate-temperature (LMT) oxidation of these fuels, as summarized in Table 1. Global properties such as LMT ignition delay times for DMF and MF were recently obtained in shock tubes and a rapid compression machine (RCM) [14,17,30]. These studies reported a complicated dependence of the relative reactivity on the fuel's molecular structure and on operating conditions [30]. More detailed information on the combustion chemistry including species profiles is quite scarce. Somers *et al*. [17] measured oxidation species profiles for DMF in a high-pressure jet-stirred reactor (JSR) at 530-1190 K. The early work of Thorton *et al*. [31] provided JSR data for furan at 1000-1300 K but did not include the mole fraction profile of acrolein, a crucial intermediate of furan oxidation. Limited species data have been reported from flow reactor experiments for DMF [32,33] and MF [34] that focused on

soot formation or on interaction with nitric oxide; fuel-specific intermediates were not provided. Similar to the sparse experimental investigations, the modeling effort for LMT oxidation of the furanics has also been quite limited. Davis and Sarathy [35] have studied OH-addition to the furan ring and Waddington-type reactions; they noted a dominant role of the ring opening reaction of the radical produced from OH-addition to the furan ring. Somers *et al.* [17] proposed a DMF mechanism that includes a treatment of some important reactions under LMT conditions. Some of these reactions such as OH-addition on DMF and H-abstractions from DMF by HO_2 were investigated using theoretical calculation methods, whereas rate constants of other important reactions such as H-abstractions from DMF by O_2 and reactions of the fuel radical with O_2, HO_2, and CH_3O_2 were still estimated at the high-pressure limit under omission of details. Xu *et al.* [30] suggested some modifications to the latest release of the Somers *et al.* model [28] by simply increasing or decreasing rate constants of some reactions to reach a reasonable agreement between model predictions and their RCM ignition delay time data of MF and DMF, an approach that cannot provide further fundamental insight.

Table 1. Main experimental studies of the LMT oxidation chemistry of DMF, MF, and furan.

Fuel	Reactor	T (K)	P (bar)	ϕ	Year & Ref.
DMF	Jet-stirred reactor (species profiles)	530-1190	10	0.5-2	2013 [17]
	Flow reactor (species profiles)	500-1400	1, 20, 40	0.03-3.33	2014 [32], 2015 [33]
	Shock tube (ignition delay times)	820-1210	20, 80	1	2013 [17]
	Rapid compression machine (ignition delay times)	737-1143	16, 30	0.5-2	2016 [30]
MF	Flow reactor (species profiles)	800-1400	1	0.02-3.33	2016 [34]
	Rapid compression machine (ignition delay times)	737-1143	16, 30	1	2016 [30]
	Shock tube (ignition delay times)	820-1215	40	1	2014 [14]
Furan	Jet-stirred reactor (species profiles)	1000-1300	1	-	1988 [31]

To the best of our knowledge, no experiment to date has addressed the quantification of species for the three unsaturated cyclic ethers furan, MF, and DMF, under identical LMT oxidation conditions. Such quantitative data is known to be very useful to analyze and understand details of the reaction mechanism in this technically relevant temperature regime. For an improved insight into the LMT

chemistry of these three furanic fuels, we have thus experimentally and numerically studied their oxidation systematically under near-identical conditions at different stoichiometries.

The paper structure is organized as follows. First, the methodologies will be described in Section 2. This section includes a description of the experimental setup (Section 2.1), the methods used in the kinetic model development (Section 2.2), as well as theoretical calculation (Section 2.3) and simulation methods (Section 2.4). Next, the results will be presented and discussed in Section 3. This section includes firstly results from the theoretical calculations and the model construction (Section 3.1), and secondly experimental results presented and discussed intertwined with the model predictions (Section 3.2). In the latter section, the fuel conversion will be described in Subsection 3.2.1, fuel-specific intermediate species in Subsection 3.2.2, and then comparisons of the formation of potential pollutants between three furanic fuels, and between flow reactor and flame in Subsection 3.2.3. Finally, a summary of the main results obtained in the present work and perspectives will be presented in Section 4.

2. Methodologies

2.1. Experiment

The oxidation of the three fuels was investigated in a laminar flow reactor at 1 bar for 9 fuel/O_2/Ar mixtures with a total flow rate of ~1.0 standard liters per minute (SLM) for three equivalence ratios (ϕ~0.5, ~1.0, ~2.0). Experimental conditions are summarized in Table 2. The experimental setup including both, reactor and mass spectrometer has been described in detail in [36-38]. The flow reactor is a fused silica tube (8 mm inner diameter, 830 mm length) that can be heated to a set temperature; it features three independent heating sections of approximately 300, 200, and 200 mm length, each monitored by a Ni–Cr/Ni thermocouple. Temperature profiles along the reactor's centerline were determined in a flow of 1 SLM pure argon for different set temperatures using a Ni–Cr/Ni thermocouple. The error in the maximum value of each temperature profile was estimated to be within 5%. However, this uncertainty for a given temperature is identical for all measured mixtures and

therefore, a relative comparison of trends between the mixtures can be performed with significantly higher precision.

The flow reactor was coupled to an electron ionization molecular-beam mass spectrometer (EI-MBMS). The gases were sampled at the reactor outlet *via* a quartz nozzle (~50 μm orifice diameter) and expanded into the 1st pumping stage, pumped to 10^{-4} mbar by a turbo-molecular pump. The formed molecular beam was further sampled by a copper skimmer at the 2nd pumping stage, and then extracted to the ionization chamber (<10^{-6} mbar). Chemical species were ionized with an electron beam of 20 eV generated by a hot-wire ionizer and accelerated into the reflectron time-of-flight (TOF) mass spectrometer (Kaesdorf) [37] with a mass resolution of $m/\Delta m$~2300 to separate the ions by their different masses. A multichannel plate was used for detection.

Table 2. Experimental conditions.

	Name of mixture	ϕ	Gas flow rate (SLM) (std. conditions: 273.15 K, 1 atm)				P (bar)
			Total	Ar	O_2	Fuel	
Furan oxidation	F0.5	0.46	0.9993	0.900	0.090	0.0093	1.0
	F1.0	0.92	0.9993	0.945	0.045	0.0093	1.0
	F2.0	1.85	0.9993	0.968	0.023	0.0093	1.0
MF oxidation	MF0.5	0.50	1.0000	0.870	0.120	0.0100	1.0
	MF1.0	1.00	1.0000	0.930	0.060	0.0100	1.0
	MF2.0	2.00	1.0000	0.960	0.030	0.0100	1.0
DMF oxidation	DMF0.5	0.53	1.0005	0.840	0.150	0.0105	1.0
	DMF1.0	1.05	1.0005	0.915	0.075	0.0105	1.0
	DMF2.0	2.10	1.0005	0.953	0.038	0.0105	1.0

The premixed gas mixtures of different equivalence ratios contained 84-96% Ar to limit self-sustaining combustion. Liquid fuels (>99%) were supplied using a syringe pump and evaporated at 393 K. Gas flow rates were metered by calibrated mass flow controllers. The gas composition was determined as a function of the reactor temperature with temperature steps of 5-6 K. The mole fraction evaluation from the obtained EI-MBMS data was then performed according to the procedures in [37,38]. The cross section of the expected dominant isomer was used for the mole fraction evaluation, relying on the guidance of previous gas chromatography (GC) results for LMT oxidation of DMF [17] and for flames [19-21]. Note that no detailed isomer analysis is available for MF and furan oxidation at LMT conditions. For those isomers for which no information was available, the most plausible

structures resulting from expected fuel decomposition pathways were assumed in a first approximation. In general, the uncertainties for reactant mole fractions are estimated to be within ±10% and those for main species (reactants, CO, CO_2, and H_2O) and directly calibrated intermediates at ±30%. Calibrations for intermediates that use the convolution of literature cross sections with the known energy distribution of the ionizing electrons are typically within a factor of 2. In the case of 5-methylfurfural for which the latter calibration method cannot be applied due to an unavailability of its ionization threshold, its calibration factor was assumed to be equal to that of furfural, and the uncertainty could therefore be higher. However, the comparison of relative trends for a specific species exhibits significant higher accuracy. The calibration method for each individual intermediate will be presented in Section 3.2.2 when discussing fuel-specific intermediates. The full data sets are available in Supplemental Material 1.

2.2 Kinetic model

In our previous studies [19-21], a single kinetic model was developed, starting from [24], for the high-temperature (HT) oxidation of DMF, MF, and furan in low-pressure flames. This model was recently extended to include the reactions of gasoline surrogate mixtures (toluene, *n*-heptane, *iso*-octane) and of polycyclic aromatic hydrocarbons (PAH) up to C_{16} [22]. As a continuous development from these studies, we have now enhanced this previous model [22], which we will call the *"HT model"* here, by including important reactions for the LMT oxidation of the furanic fuels to derive the new *"LMT model*" in the present work. While the main features of this LMT model and important additions and changes will be described in more detail in Section 3.1, the methodology for the model development will be addressed here. Please note that structures and names of species discussed in this paper are available in Table S1 in Supplemental Material 2.

Important reaction paths of fuel consumption and of the formation of primary products were first identified from rate-of-production (ROP) and sensitivity analyses for the studied conditions and then examined against the detected species in the present LMT measurements. In MF oxidation, for example, species with a mass-to-charge ratio *m/z*=96 were detected with a high mole fraction already

at the lowest temperatures; this observation is in agreement with the ROP analysis for MF oxidation that shows furfural (*m/z*=96) to be largely produced by the reaction of the fuel radical 2-furylmethyl (MF-yl) with the HO_2 radical. Also, bimolecular initiation reactions of DMF and MF with O_2 were found from sensitivity analyses to notably influence the systems' reactivity under the present LMT conditions.

For reactions identified as important from these examinations, theoretical computation methods described in Section 2.3 below were employed with an aim to obtain kinetic data of improved accuracy. Also, potentially missing reaction classes were identified using existing knowledge on the oxidation of species with similar structure as well as indications from the experimentally detected species. For example, MF and DMF reactions are similar to toluene chemistry because all molecules are methyl-substituted aromatic species and the methyl group is expected to be the most reactive moiety. Similarly, resonance-stabilized benzyl radical (C_7H_7) reactions, *e.g.* with O_2 and HO_2 studied in [39,40], are considered to be representative for the analogous furylmethyl reactions. Then, rate constants of the potentially missing reactions were first estimated so that they could be added into the model to check their influence. Whenever such reaction classes were seen to play a role under the studied conditions, they were then investigated in depth with the theoretical computation methods to explore plausible pathways and calculate their kinetic data. As an example, the present DMF experiments showed a very fast rise of the formaldehyde mole fraction with increasing temperature, indicating that this carbonyl species could be an important product for LMT conditions. This observation was found to be consistent with the theoretical calculations that identified the addition of O_2 to the fuel radical, 5-methyl-2-furanylmethyl (DMF-yl), as a plausible path of formaldehyde formation in DMF oxidation, as we will discuss more intensively in Section 3.

Priority was thus given to improve the model systematically by including results from detailed high-level theoretical calculations for selected reactions of which notable influence was expected, especially for primary reactions of the furanic fuels. When rate constants from theoretical calculations were not available, they were estimated by analogy with species of similar structure or based on rate rules [41-43] and included into the LMT model. Those methods were applied mostly for the secondary

mechanism, such as subsequent reactions of methyl vinyl ketone, 5-methylfurfural, furfural, 2-ethyl-5-methylfuran, and 2-ethylfuran. The present model contains detailed reactions for these latter species, such as unimolecular initiation, H-abstraction, H- and OH-addition reactions to double bonds, and subsequent decomposition of the created radicals.

Most thermochemical data for newly-involved species were taken from quantum chemistry calculations in the present work or relied on recent results from the literature [17,27,28]. Otherwise, such data was calculated using the software THERGAS [44] that is based on the group additivity method proposed by Benson [45]. Transport properties of newly-involved species were estimated based on the correlation proposed by Wang and Frenklach [46]. Theses authors used the boiling temperatures, critical temperatures, and critical pressures of a large number of selected species to develop a relation between molecular weight (M_w) and Lennard-Jones collision diameter (σ) and potential well-depth (ε/k_B). The two latter parameters serve as input to simulation code to compute the transport properties of each species. As a first approximation, this well-established correlation has been used in the present work to estimate σ and ε/k_B for newly-involved species for which no data is available in the literature. While the effects of transport properties can be neglected in the simulations of the present LMT flow reactor, these properties could play an important role when the model is used for simulating flame systems. Therefore, sensitivity analyses of the flame propagation and flame speciation to the transport data has been performed exemplarily for DMF in air at ϕ=1, 1 bar, and initial temperature of 298 K as selected conditions. The results indicated that an increase or a decrease (by a factor of 2) of σ and ε/k_B of any species created by LMT reaction paths (as detailed in Section 3.1) does not affect the flame speeds or the flame species profiles. Only the Lennard-Jones parameters of fuel (DMF) and its corresponding radical (DMF-yl) have a slight impact on flame speeds and the maximum mole fractions of primary species (1-3% when increasing or decreasing σ and ε/k_B of these species by a factor of 2). The σ and ε/k_B of DMF and DMF-yl used in the present model are found to be very close to those of the literature [17,43] (difference <10%), therefore the correlation of Wang and Frenklach [46] is expected to provide transport data accurate enough for the purpose of this study. Note that the sensitivity analysis indicated that the transport data of oxidizers (O_2/N_2), CO, and small

radicals (H, OH, O) affect flame speeds strongly (up to 60% in the case of N_2), however detailed analyses of the uncertainty of the transport data of these database species are beyond the scope of the present study.

2.3 Theoretical calculations

To well address reactions that may strongly affect the LMT oxidation of furanic fuels, thermodynamic properties of related molecules and rate coefficients for several reactions of MF and DMF were calculated with quantum mechanical and statistical methods.

First, electronic structure calculations at the CBS-QB3 level of theory [47] were performed using the Gaussian 09 revision D suite of programs [48]. Using well-established relationships between molecular properties and partition and thermodynamic functions from statistical mechanics, the output of the *ab initio* calculations was used to determine the thermodynamic properties of reactants, products, and transition states. The electronic energies were converted with the atomization method [49] to the corresponding heats of formation. B3LYP/6-311G(d,p) level rotational constants and scaled (factor 0.99) harmonic frequencies, except for those that represent internal rotations, were used to calculate the thermal contributions to the enthalpies as well as entropies and heat capacities. Hindrance potentials of internal rotors that are not well described as harmonic oscillators were determined *via* relaxed scans by increasing the corresponding dihedral angle in 10 degrees steps until complete rotation was achieved. These potentials were regressed to Fourier series prior to their use. The reduced moments of inertia were calculated at the $I^{(2,3)}$ level as defined by East and Radom [50]. With this information, the Schrödinger equation for one-dimensional axis-fixed rotation could be solved, and the resulting energy eigenvalues were employed to calculate the contributions of these modes to the thermodynamic functions. Finally, the thermodynamic data was stored in form of NASA polynomials.

The CBS-QB3 composite method uses DFT calculations at the B3LYP/CBSB7 level to determine the optimized structure and frequencies of a species. While those geometries are generally of good accuracy for most regular molecules and for tight transition states, they tend to be less accurate for

loose transition states. In the current work, the transition states for HO_2- or O_2-additions to the resonance-stabilized fuel radicals, *i.e.* 2-furylmethyl (MF-yl) and 5-methyl-2-furanylmethyl (DMF-yl), are quite loose, and the geometries and frequencies for these reactions were therefore determined at the QCISD/6-31G(d) level of theory. The QCISD/6-31G(d) structure was subsequently used in the CBS-QB3 calculation using an IOP command in the Gaussian software to suppress the B3LYP geometry optimization. In the following, we will refer to this modified CBS-QB3 method as QCBS-QB3. The QCBS-QB3 calculations were only used to calculate rate coefficients, while the original CBS-QB3 method was also utilized to derive thermodynamic properties after applying bond additive corrections (BAC) to account for systematic errors in the electronic structure calculations [51,52]. The BAC data were derived by comparing uncorrected CBS-QB3 results for selected molecules to accurate experimental data. Note that BAC are not used for kinetic calculations which only require relative energies. However, rate coefficient calculations require that all energies are obtained at the same level of theory, *e.g.*, when using the QCBS-QB3 method for rate coefficient calculations, all reactants, products, and transition states need to be calculated at this level.

In the second step, transition state theory expressed in terms of Gibbs free energies was used to calculate the rate coefficients:

$$k_{TST}(T) = \chi(T) \cdot \frac{k_B T}{h} \cdot \left(\frac{RT}{p}\right)^{\Delta n - 1} \cdot e^{-\frac{\Delta G^{\ddagger}}{RT}}$$

here $\Delta G^{\ddagger}$ is the Gibbs free energy difference between transition state without the transitional mode and reactant(s), Δn is the molecularity of the reaction, and $\chi(T)$ is a correction factor that accounts for quantum mechanical tunneling. The asymmetric Eckart potential was used in this work to calculate $\chi(T)$. The Gibbs free energies were obtained from the NASA polynomials calculated in the first step. Rate coefficients were calculated for temperatures ranging between 300 K and 2500 K in 50 K steps. The individual rate coefficients were finally regressed to modified Arrhenius expressions.

Bond scission reactions of peroxide molecules (ROOH) – *i.e.* products of the HO_2 recombination with the MF-yl and DMF-yl radicals – proceed through transition states with no pronounced barriers, hence one would have to use variational transition state theory to calculate rate expressions. Such

calculations are tedious, and the possibility for the leaving OH moiety to form an H-bond with the furanic oxygen creates additional problems. Therefore, we chose to estimate the rate expressions for these reactions based on the average rate coefficient for methyl peroxide dissociation taken from the NIST chemical kinetics database [53] and the benzylhydroperoxide dissociation rate coefficient by da Silva and Bozzelli [39]. Using the CBS-QB3-based equilibrium constants, the reverse rate coefficients of both reactions were calculated, and the average value was used as an estimate for all RO + OH association reactions considered in the present study. The corresponding O–O bond scission rate expressions were again obtained from microscopic reversibility.

Finally, pressure-dependent rate coefficients for the addition of O_2 and HO_2 to MF-yl and DMF-yl radicals were established with the QRRK method developed by Dean and co-workers and implemented in the code ChemDis [54,55]. Although more sophisticated software tools are available, past experience showed that the simpler QRRK approach leads to comparable results [56]. The pressure-dependence analysis was carried out for 500-2500 K and 0.01-100 bar using Ar as the bath gas. The Lennard-Jones parameters for the addition products were approximated with the values of benzene. Note that previous studies using the same method showed that the results are not very sensitive to the choice of these parameters [56]. Furthermore, these parameters of benzene are very close to those estimated for individual studied species [46] (within 20% differences). The ΔE_{all} value (average energy transferred by a collision) for Ar was taken as -334 cal mol^{-1}, which is the default value for argon provided by the program. The results were regressed for each pressure to modified Arrhenius expressions. Only the major reaction pathways were included in the pressure-dependence analysis, minor ones were omitted, as will be discussed in more detail in Section 3.1.

The enthalpies calculated at the CBS-QB3 level of theory are generally accurate to 1 kcal mol^{-1} and rate coefficients for reactions processing through well-defined (tight) transition states are expected to be within a factor of 2 to the correct value. However, that of O_2-addition to the fuel radicals and ROOH dissociation are expected to be slightly higher (within a factor of 3) because the transition states are quite loose as mentioned earlier. This order of uncertainty is considered for HO_2-addition to the fuel radicals. However, an additional source of uncertainty could be taken into account for the HO_2-

addition reactions because these reactions to the fuel radials proceed likely through initial van-der-Waals complexes, which were, however, not considered in the rate coefficient calculations. Therefore, total uncertainty in the rate coefficients of these reactions could be as high as a factor of 5.

2.4 Simulation method

Simulations of the present flow reactor data were performed using the plug-flow reactor (PFR) module of the LOGESoft package [57]. To account for the potential heat release from the mixture during oxidation, a linear heat transfer coefficient was assigned in the simulations following the approach in [38]. For this, the reactor was divided into three zones: (1) a heating zone where the gas is heated to the reactor temperature, (2) the reaction zone at the set temperature of the reactor that includes heat released by the reactive mixture, and (3) a cooling zone. A python code [58] was written to forward the results from a previous zone as input parameters to the next zone. From the measured temperature profiles with 1 SLM of pure argon as validation, the heat transfer coefficient was estimated to be 10 W $m^{-2}K^{-1}$, with an uncertainty of 5%. To assess a potential influence of heat release on the simulation results, measured and calculated temperature profiles at different set temperatures in a non-reactive flow of pure Ar were compared against simulations for the DMF1.0 mixture of Table 2 at these temperatures, see Fig. S1 (Supplemental Material 2). A very rapid temperature increase is observed when self-sustaining combustion occurs, *i.e.* at the highest temperatures studied, which for stoichiometric conditions and DMF is above ~990 K. Similarly, this phenomenon was observed for MF and furan above ~970 K, with a moderate dependence of this threshold also on equivalence ratio for all three fuels. Up to these temperatures, Fig. S1 demonstrates very good agreement of the simulations for the reactive mixture with the measurements in the non-reactive case. It was examined whether the occurrence of self-sustaining combustion in the high-temperature range would affect the simulated species profiles. Figure S2 provides an exemplary comparison of an isothermal simulation (using the temperature profile of the non-reactive case) with the modeling results using the estimated heat transfer coefficient of 10 W m^{-2} K^{-1}. While differences are not dramatic, some influences are seen in the high-temperature region near and above ~950 K. We believe that taking into account the

possible heat release from the reactive mixture during oxidation is more reasonable in view of the experimental observations at high temperatures, and have thus applied the non-isothermal approach throughout.

3. Results and discussion

Theoretical calculation and model construction results will be presented in Section 3.1. Experimental results will be discussed in detail in Section 3.2 together with model predictions and analyses. Special emphasis will be placed on the fuel conversion behavior, on the nature and mole fractions of fuel-specific intermediate species, and on the formation of potential pollutants.

3.1. Theoretical calculation and model construction results

With the approach described above, a reaction mechanism including 3145 elementary reactions among 524 chemical species (including PAH species) was composed that encompasses LMT and HT oxidation of furan, MF, and DMF. This mechanism is available in CHEMKIN format together with thermodynamic and transport properties in Supplemental Material 3. Each species is labeled with its IUPAC International Chemical Identifier (InChI) to allow for unambiguous identification of the molecular structure. In the LMT model presented here, the Pressure Dependence Through Logarithmic Interpolation function (PLOG) was used to represent pressure-dependent rate expressions. The performance of this model was examined against the present LMT experiments as well as selected data sets taken from the literature. Overall, the data cover LMT and HT conditions for a range of pressures between 20 mbar at the low and 80 bar at the high end. Results of these performance tests are presented in Figs. S3-S11 (Supplemental Material 2).

Specifically, these selected LMT data include species-resolved JSR data for DMF at 10 bar [17] (Fig. S3), some species profiles measured in a flow reactor for MF at 1 bar [34] (Fig. S5), and earlier results for furan in a JSR at 1 bar [31] (Fig. S7). Also, global properties in the LMT regime include shock tube ignition delay times for DMF at 20 and 80 bar [17] (Fig. S4) and RCM ignition delay times of MF at 16 and 30 bar [30] (Fig. S6). The HT data include low-pressure flame experiments of DMF, MF, and furan [19-21] (Figs. S8-S10), and shock tube ignition delay times at 1.2-16 bar [25] (Fig.

S11). In general, satisfactory agreement is observed between literature experiments and predictions with the new LMT model.

With the HT model that was extensively described in the previous studies [19-22,24] as a basis, the most important developments in the LMT oxidation include theoretical calculations of the rate coefficients for the following sets of reactions: H-abstractions from the lateral methyl groups of DMF and MF by O_2 and reactions of the resonance-stabilized fuel radicals 2-furylmethyl (MF-yl) and 5-methyl-2-furanylmethyl (DMF-yl) with HO_2 and O_2. The results of these calculations will be presented point-by-point in the following sections. Finally, additional important reactions that were changed in the model will be described.

3.1.1. H-abstractions from the lateral methyl groups by O_2

A preliminary analysis with the HT model [22] indicated that H-abstractions from the lateral methyl groups of DMF and MF by O_2 strongly affect the conversion of these fuels under LMT conditions, pointing to the need for good kinetic data for these reactions. Since their rate coefficients were only estimated in previous work, we have now used quantum chemistry computations for their calculation. The resulting Arrhenius expressions (in cm^3, mol, s, cal units) for the reactions:

$DMF + O_2 \leftrightarrows HO_2 + DMF\text{-}yl$ (R1)

and

$MF + O_2 \leftrightarrows HO_2 + MF\text{-}yl$ (R2)

are $k=2.9\times10^2T^{3.34}\exp(-33300/RT)$ and $k=1.6\times10^2T^{3.34}\exp(-34700/RT)$, respectively. Figure 1 presents these rate coefficients as a function of temperature. With an ~1 kcal mol^{-1} lower barrier for the DMF *versus* the MF reaction, combined with the appropriate statistical factor of 2, the rate coefficient for R1 is ~4 times larger (in the studied temperature range) than that for R2. Figure 1 includes the rate coefficients used in the model of Somers *et al.* [28] and in our previous HT model [22]. In the model of Somers *et al.* [28], the rate coefficients for DMF were estimated based on an Evans-Polanyi relationship, while that of MF relied on an estimated rate expression based on those for DMF and toluene. The rate coefficients used in our previous HT model [22] were estimated using

EXGAS rate rules [41] with a pre-exponential factor of 7E+11 (in cm^3, mol, s units) and an activation energy assumed as being equal to the enthalpy of reaction at 800 K. Significant differences are seen of up to an order of magnitude in the temperature range 700-1100 K, with deviations of earlier estimations from the present calculations noted in both directions. We expect the rate coefficients calculated in the present work to be more accurate and included those in the LMT model to improve its prediction capability. Note that due to the low bond dissociation energies (BDE) of C─H at the allylic position, the rates of H-abstractions from the lateral methyl groups of MF and DMF are, for temperatures of interest, at least two to four orders of magnitude higher than those recommended for alkanes and benzene (see in the core model or in [28]).

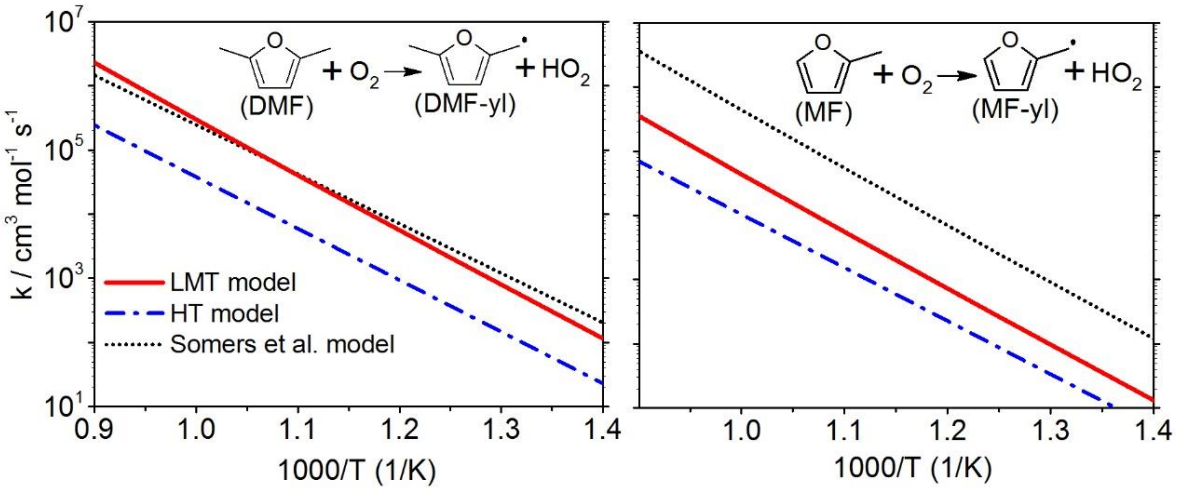

Figure 1. Rate coefficients of H-abstractions from MF and DMF by O_2 calculated in the present work and used in the present LMT model, compared with those estimated and used in the Somers *et al.* model [28], and with those estimated by EXGAS software [41] used in our previously published HT model [22].

3.1.2. Reactions of resonance-stabilized fuel radicals with HO_2

The bimolecular reactions of the HO_2 radical with the resonance-stabilized fuel radicals MF-yl and DMF-yl lead to the formation of a reactive OH radical. Therefore, they should be very important, especially at LMT conditions at which unimolecular decomposition of the fuel radicals is slow. We therefore examined these reactions in detail using the computational methods described above. While the potential energy surfaces (PES) and the optimized geometries of related species are available in

Supplemental Material 2 (Fig. S12 and Table S3, respectively), possible reaction pathways of MF-yl and DMF-yl with HO_2 are presented in Fig. 2, together with rate coefficients calculated at 940 K.

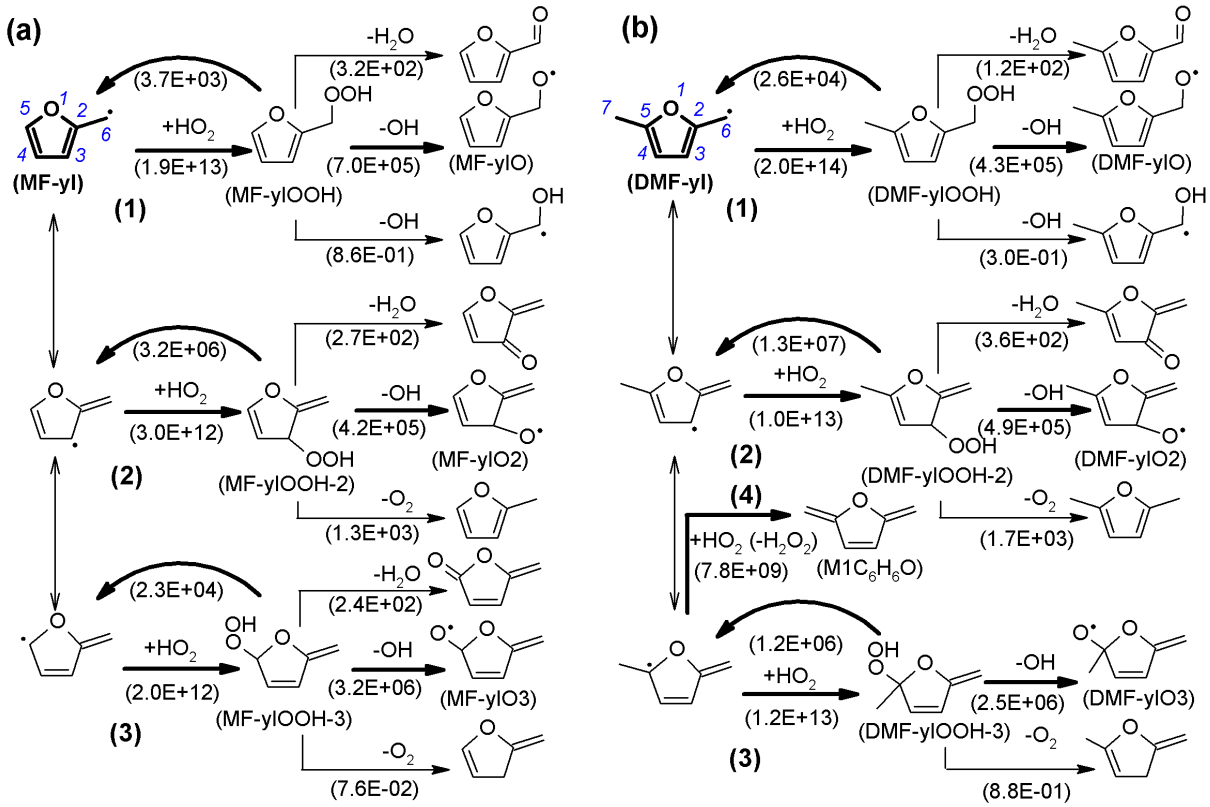

Figure 2. Pathways of the bimolecular reactions of the resonance-stabilized 2-furylmethyl (MF-yl) and 5-methyl-2-furanylmethyl (DMF-yl) radicals with the HO_2 radical. Thick arrows denote major channels that were included in the pressure dependence analysis. Below the arrows, rate constants calculated at 940 K are provided.

Because MF-yl and DMF-yl radicals are resonance-stabilized, HO_2 can combine to three distinct sites, *i.e.* at the CH_2 moiety, and in C3 and C5 position (positions are identified with italic numbers in Fig. 2). As shown in Fig. 2, HO_2-addition to the CH_2 moiety (channel **1**) is faster than the two other options (channels **2** and **3**). The peroxide product of channel **1** is more stable than those of channels **2** and **3** as indicated in Fig. S12. The O–O bond of peroxide species, MF-ylOOH and MF-ylOOH-3 *versus* DMF-ylOOH and DMF-ylOOH-3 produced by channels **1** and **3**, respectively, breaks faster than the re-dissociation of the adduct to fuel radical + HO_2. These channels thus play an important role in converting a rather unreactive HO_2 to a reactive OH radical. The opposite situation is found for the peroxide species MF-ylOOH-2 and DMF-ylOOH-2 produced by channels **2**, because their re-

dissociation dominates, compared to other decomposition paths. From cleavage of the O–O bonds of all these peroxide species, OH radicals are formed, and these reactions were identified as major channels because their rate coefficients (order of magnitude E+05 to E+06) are much higher than other forward dissociation pathways such as elimination of H_2O or O_2, and formation of an alcohol radical (order of magnitude E-02 to E+02) (Fig. 2). These observations on rates are consistent with barriers calculated for these reaction paths (Fig. S12), here the cleavage of the O–O bond is energetically favored. Note that due to the availability of a second lateral methyl group, an additional pathway, *i.e.* H-abstraction from DMF-yl by HO_2, was identified for DMF-yl (channel **4**) that does not exist for MF-yl. The rate coefficient of this reaction was also computed and included in the LMT model. All major channels are highlighted with thick arrows in Fig. 2. While the minor channels were omitted in the model to avoid complexity and additional uncertainty, the major ones were considered in the model and included in the pressure dependence calculations. The pressure-dependent rate coefficients (pressure range of 0.01-100 bar) together with high-pressure limiting ones are available in Supplemental Material 4. Such detail of reactions of MF-yl and DMF-yl with HO_2 is one of the distinguishing features of the present LMT model. Earlier models for the furanic fuels including our previously published HT model [19-22] and that of Somers *et al.* [17,27,28] considered only channel **1** without pressure dependence, and rate coefficients were only estimated. Note that according to the pressure-dependence analysis in the present study, the reactions of MF-yl or DMF-yl with HO_2 were found to be strongly influenced by pressure. Exemplarily, when the pressure increases from 1 bar to 100 bar, the rates of reaction MF-yl + HO_2 = MF-ylOOH and those of DMF-yl + HO_2 = DMF-ylOOH increase by factors of 4-12 (in the temperature range of 800-1100 K).

To replace the estimates in the HT model [22], we have also theoretically calculated the kinetic data of the subsequent reaction subset of the MF-ylO radical for the first time, and – because of the similar structure and close BDE of $C_{lateral}$─H and $C_{lateral}$─C_{ring} between MF-ylO and DMF-ylO – we have applied the rate coefficients computed for MF-ylO also for DMF-ylO without any modification as a first approximation. MF-ylO (or DMF-ylO) radicals can be consumed by several reactions (not shown in Fig. 2): (**i**) by C–H β-scission to produce H + furfural ($C_5H_4O_2$) or 5-methylfurfural

($C_6H_6O_2$), (**ii**) by C–C β-scission yielding furyl (furyl-2) or 5-methylfuryl (MF-yl-2) radicals + formaldehyde (CH_2O), and (**iii**) by isomerization to produce the radicals 2,3-dihydrofurfural-yl (MF23HCHO) or 2,3-dihydro-5-methylfurfural-yl (DMF23HCHO). The resulting Arrhenius expressions (in cm^3, mol, s, cal units) for reactions (**i**)–(**iii**) are $k_i=1.2\times10^{9}T^{1.44}exp(-17300/RT)$, $k_{ii}=2.9\times10^{14}T^{0.14}exp(-31900/RT)$ and $k_{iii}=4.3\times10^{8}T^{1.22}exp(-16700/RT)$, respectively (see also Supplemental Material 4). It should be noted that the reaction (**i**) is about 10-50 times faster than the two others in the studied temperature range because the $C_{lateral}$─H bond (BDE ~11 kcal mol^{-1}) is much weaker than the $C_{lateral}$─C_{ring} bond (BDE ~29 kcal mol^{-1}), and most importantly, that the theoretical results obtained here are factors of 200-500 higher than the previous estimates [19-22] in the LMT regime.

3.1.3. Reactions of resonance-stabilized fuel radicals with O_2

Oxygen addition to the fuel radicals has been recognized as an important reaction class in LMT oxidation, associated with a high amount of formaldehyde that was detected here at low DMF and MF conversion. This experimental result motivated us to investigate this reaction class more profoundly. We have identified major pathways for O_2-addition to MF-yl and DMF-yl radicals that can occur at the same three sites (*i.e.* CH_2 moiety, C3 and C5 positions) that were discussed above for HO_2-addition. PES investigations showed that the MF-ylOO radical produced by O_2-addition to the CH_2 moiety is sufficiently stable with respect to re-dissociation that isomerization and product channels become competitive. Moreover, the adducts formed by O_2-addition to the C3 and C5 positions are considerably less stable and re-dissociation completely dominates, any product formation channel. More details of the PES and the optimized geometries can be found in Fig. S13 and Table S3 of Supplemental Material 2. Possible pathways for MF-ylOO and DMF-ylOO are shown in Fig. 3.

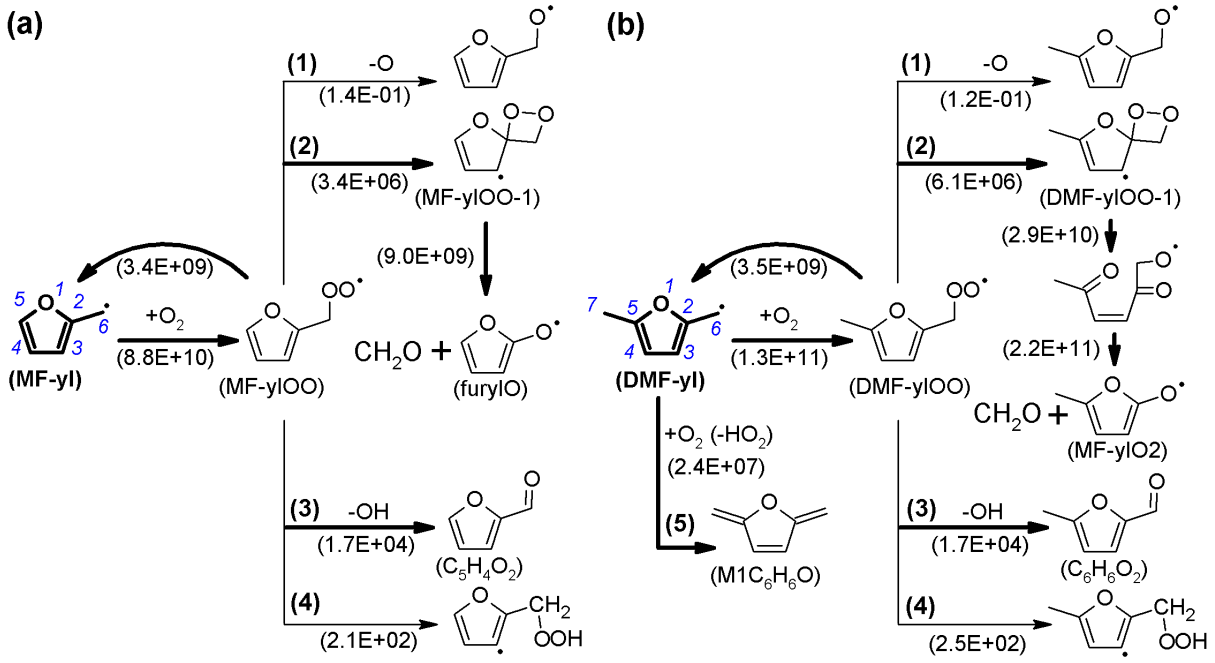

Figure 3. Pathways of the bimolecular reaction of MF-yl and DMF-yl with O_2. Thick arrows denote major channels that were included in the pressure dependence analysis. Below the arrows, rate constants calculated at 940 K are provided.

As indicated in Fig. 3, O_2-addition to MF-yl or DMF-yl to yield furanylperoxy (MF-ylOO) or methylfuranylperoxy (DMF-ylOO) radicals proceed with rate coefficients of around 1E+11. Among the decomposition pathways of the adducts, re-dissociation dominates any other channel by at least three orders of magnitude. Nevertheless, re-dissociation and subsequent adduct formation create a quasi-steady state concentration of the adduct. Therefore, even if a product channel of the adduct is much slower than re-dissociation, it could be become important if it is essentially irreversible because it acts as an outlet for the quasi-steady state system. Among product channels, channels **1** and **4** are much slower than channels **2** and **3** (Fig. 3) because channels **2** and **3** are energetically favored with barriers about 4-40 kcal mol^{-1} lower than channels **1** and **4** as showed in Fig. S13. Channel **2** is an interesting option because it has a barrier much lower than those of other forward dissociation channels (Fig. S13) and leads to the highly reactive spiro intermediates MF-ylOO-1 and DMF-ylOO-1. Although their formation is three orders of magnitude slower than re-dissociation of MF-ylOO or DMF-ylOO (Fig. 3), they still consume the peroxy adduct and produce formaldehyde and furanyloxy (furylO) or methylfuranyloxy (MF-ylO2) radicals, respectively. Interestingly, it was found that in case of MF-ylOO-1, formaldehyde (CH_2O) was directly formed from the spiro intermediate. This is not

the case for DMF-ylOO-1 because the corresponding spiro intermediate prefers to ring-open rather than to eliminate CH_2O. Still this sequence ultimately leads also to the formation of CH_2O. Channel **3** leads to OH + furfural (for MF) or methylfurfural (for DMF). Although the rate coefficients are two orders of magnitude lower than for the competing channel **2**, the reaction could play a role because OH is formed. The current analysis agrees qualitatively with a theoretical study by Simmie and Metcalfe [59] for channels **3** and **4**. However, these researchers did not take the important CH_2O elimination (channel **2**) into account. Also, it is interesting to compare the theoretical analysis by Murakami *et al.* [40] for the structurally similar benzyl radical, resulting in an analogous reaction system to that suggested here. While the minor channels **1** and **4** were omitted in the present model to reduce its complexity, the major ones denoted by thick arrows in Fig. 3 were included in the model considering pressure-dependent rate constants for range of 0.01-100 bar. Note that the reactions of MF-yl and DMF-yl with O_2 were found to depend strongly on pressure; their rates increase by factors of 15-50 when increasing pressure from 1 bar to 100 bar. Because of the availability of a second lateral methyl group, already discussed above for the case of DMF-yl + HO_2 (Section 3.1.2.), H-abstraction from DMF-yl by O_2 (channel **5** in Fig. 3) was also included in the model. All pressure-dependent rate coefficients of the reaction systems MF-yl + O_2 and DMF-yl + O_2 are provided in Supplemental Material 4.

3.1.4. Other primary reactions relevant for LMT conditions

It was noted that the reaction of DMF-yl + CH_3O_2 potentially influences the reactivity of the DMF oxidation under LMT conditions [17]. The main channels for the DMF-yl and MF-yl + CH_3O_2 systems were thus included in the model, considering again that CH_3O_2 can add to the three sites (CH_2 moiety, C3 and C5 positions) of the resonance-stabilized MF-yl and DMF-yl radicals. The rate coefficients are assumed to be the same as those for the analogous reactions with HO_2.

Furthermore, recombination of DMF-yl and MF-yl with CH_3, forming 2-ethyl-5-methylfuran (MEF) and 2-ethylfuran (EF), respectively, contributes to the consumption of these fuel radicals and thus affects the overall reactivity at LMT conditions. These recombination reactions were not included

in our previous HT model [22], and were now added with rate coefficients estimated from the recombination of CH_3 with the resonance-stabilized allyl radical [60]. The detailed reaction subsets for MEF and EF consumption were also added, with kinetic data mainly estimated by analogy to DMF and MF.

A preliminary analysis indicated that OH-addition to the furan ring largely contributed to the consumption of DMF, MF, and furan at the studied LMT conditions. Moreover, potential products of this process such as acrolein (C_3H_4O) and methyl vinyl ketone (C_4H_6O) were experimentally detected with high mole fractions. Therefore, more accurate kinetic data than the estimated ones used in the HT model [22] were needed. The present LMT model has adopted reaction pathways and kinetics for OH-addition to MF and DMF from the recent CBS-APNO and G3 calculations by Somers *et al.* [17,27,28], and for OH-addition to furan from the CCSD(full)/6–311+G(3df,2p) computations by Mousavipour *et al.* [61].

Additionally, the MF sub-mechanism was improved by replacing previous estimates [22] for ring opening reactions of the MF-yl radical, H-addition reactions, unimolecular initiation reactions, and H-abstractions from MF by H and CH_3 with recently calculated rate coefficients from quantum chemical methods [28].

Finally, the furan sub-mechanism now includes the kinetic data for H-abstractions from furan by OH from the theoretical calculations of Mousavipour *et al.* [61]. H-abstractions by H and CH_3 were estimated based on theoretical calculations for such reactions at the C5 position of MF [28,35] to replace the kinetic data based on alkenes in the HT model [22]. For H-abstractions by HO_2 and CH_3O_2, two approaches were tested that will be discussed further below. In the first case, the kinetic data of these reactions was taken from the RMG database [43], whereas in the second case, the present theoretical calculation results for H-abstraction from the C3 position of furan by HO_2 were adopted as a first approximation for H-abstractions by HO_2 and CH_3O_2 at all carbon sites of furan.

Reactions of fuel radicals (furyl-2, C_4H_5O-2, and furyl-3, C_4H_5O-3) with HO_2 and CH_3O_2 were also considered and written as global reactions with estimated rate coefficients based on similar reactions of alkenyl radicals within the C_3-C_4 sub-mechanism in the core model. Since we observed

that these reactions have no important role in controlling the oxidation behavior of furan at the present LMT conditions, we abstained from performing further theoretical calculations to improve their kinetic data.

3.2. Experimental and model prediction results

About 35 species including reactants, intermediates, and products in the mass range up to *m/z*=128 were quantified in this study by EI-MBMS. After a discussion of the fuel conversion behavior, a detailed analysis of the most important intermediate species will be given, followed by an assessment of the formation of potential pollutants.

3.2.1. Fuel conversion

Figure 4 presents the mole fraction profiles of DMF, MF, and furan as function of temperature together with predictions with the present LMT model. All three fuels start to react in the 750-900 K range and are completely converted at 950-1100 K, depending on the fuel and equivalence ratio. In general, DMF conversion starts at lower temperatures compared to MF and furan in particular, which starts to react only at ~950 K. The width of the reaction zone decreases significantly from DMF to furan. As expected, the reaction zone shifts to lower temperatures with leaner mixtures, especially for DMF. NTC behavior was not clearly observed and no fuel consumption was detected experimentally below 700 K. An increasing dependence of the fuel conversion on equivalence ratio from furan to DMF is evident from in Fig. 4, a trend that seems to correspond with the number of lateral methyl groups in the fuel molecule. This behavior points to the importance of bimolecular initiation reaction with O_2 for DMF and MF conversion, whereas these reaction classes seem less important for furan conversion. Despite of some remaining deviations in the absolute values, the model predicts these experimentally observed trends quite well. For example, the experimental observation that DMF is consumed much faster under lean conditions than for the other equivalence ratios is in agreement with the JSR experiment of Somers *et al.* [17], and the LMT model predicts this behavior successfully (Figs. 4 and S3). According to sensitivity analyses, besides the H-abstraction reactions by O_2, the reaction DMF-yl + O_2 ⇆ MF-ylO2 + CH_2O was found to also strongly promote DMF conversion, because the ring

opening of the MF-ylO2 radical leads ultimately to the formation of CH_3CO which in turn supplies the CH_3 radical to the system. The balance of the CH_3 and O_2 mole fractions and the respective reaction channels will have a sensitive influence on the net consumption for the different stoichiometries, contributing to the different reactivity of the system. In the case of MF, the analogous reaction, *i.e.* MF-yl + O_2 ⇆ furylO + CH_2O, still consumes the fuel radical (MF-yl), but cannot release the CH_3 radical due to an absence of the second lateral CH_3 group in the furylO structure. Under the fuel-lean condition, the reactivity could therefore be inhibited by this reaction, resulting in a different reactivity behavior (Fig. 4b). In the case of furan, the lack of lateral methyl groups limits the role of abstraction reactions and thus the contribution of the created fuel radicals for controlling the system reactivity, and therefore the dependence of the reactivity of furan on the equivalence ratio is very slight. The present model reproduces this behavior very well.

At comparatively high fuel conversions, *i.e.* high temperatures (above ~1000 K for the DMF2.0 mixture and above ~980 K for the MF2.0 mixture) the LMT model starts to over-predict the fuel consumption (Fig. 4a,b), and therefore the simulated mole fraction profiles are slightly shifted to lower temperatures *versus* the experimental profiles, a potential influence of self-sustaining combustion as discussed above (Section 2.4). Mole fraction profiles of the major species O_2, CO, CO_2, and H_2O involved in the global fuel conversion are available in Figs. S14-S16 (Supplemental Material 2). As expected, both experiment and simulation show that CO, CO_2, and H_2O are produced in large amounts. Mole fractions of the two latter species increase with temperature and reach maximum values at highest fuel conversion, while for the fuel-lean and stoichiometric mixtures, the CO mole fractions reach maxima at intermediate temperatures.

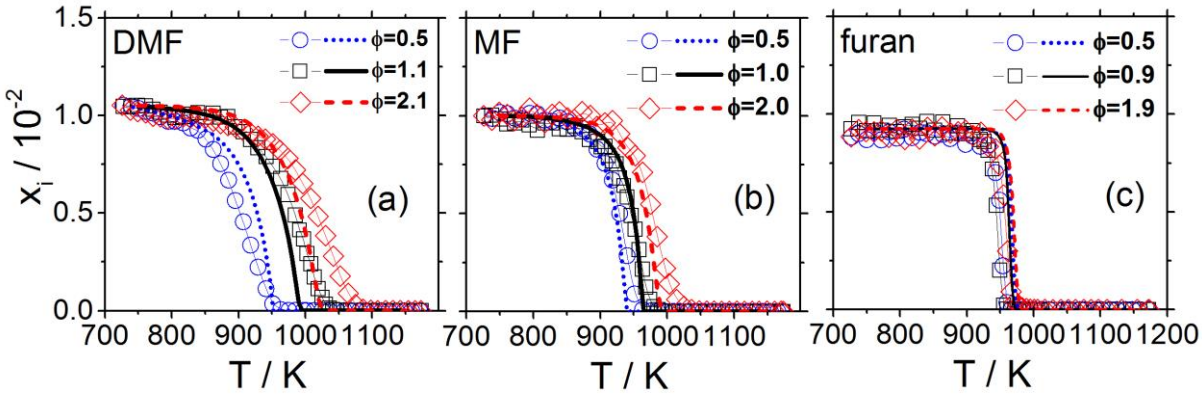

Figure 4. Fuel mole fractions as a function of reactor temperature. *Symbols:* experiment; *lines:* LMT model.

3.2.2. Fuel-specific intermediate species

An overview of the mole fractions of intermediate species detected in the oxidation of the three fuels is presented in Table 3 for ϕ~1.0 (*i.e.* mixtures DMF1.0, MF1.0, F1.0); maximum mole fractions are reported together with the temperatures at which they occur. Data for the three equivalence ratios studied for DMF, MF, and furan oxidation are given in Tables S4, S5, and S6 in Supplemental Material 2, respectively, to facilitate an overall comparison.

Table 3. Intermediate species mole fractions for the oxidation of furanic fuels at ϕ~1.0, determined experimentally by EI-MBMS at an ionization energy of 20 eV. Nomenclature: **M**: nominal mass; **IP**: ionization threshold (in eV). Calibration method: **a:** direct cold gas calibration, **b**: convolution of energy distribution and ionization cross section, **c**: as furfural. $\mathbf{x_{max}}$: peak mole fraction, $\mathbf{T(x_{max})}$: temperature at $\mathbf{x_{max}}$. Identification of the expected dominant isomer was based on the guidance of previous GC results for LMT oxidation of DMF [17] and for flames [19-21] when possible, otherwise the most plausible structures resulting from expected fuel decomposition pathways were assumed in a first approximation.

Species	M	IP	Calib.	Calibrated as	DMF		MF		Furan	
					x_{max}	$T(x_{max})$	x_{max}	$T(x_{max})$	x_{max}	$T(x_{max})$
CH_4	16	12.60	a	Methane	3.2E-3	1047	1.8E-3	986	6.1E-4	955
C_2H_2	26	11.40	a	Acetylene	8.0E-4	1041	5.6E-4	980	9.2E-4	955
C_2H_4	28	10.51	a	Ethylene	4.4E-3	1047	4.0E-3	986	1.8E-3	955
CH_2O	30	10.88	b	Formaldehyde	1.4E-3	1030	1.5E-3	968	1.1E-3	949
C_2H_6	30	11.52	a	Ethane	5.3E-4	1030	5.2E-4	968	7.4E-4	949
C_2H_2O	42	9.62	b	Ketene	3.4E-4	1025	2.1E-4	968	8.9E-5	949
C_3H_6	42	9.73	a	Propene	6.0E-4	1030	3.9E-4	968	3.9E-5	955
C_4H_2	50	10.17	b	Diacetylene	1.9E-5	1025	7.3E-6	968	3.4E-6	949
C_4H_4	52	9.58	b	Vinylacetylene	1.1E-4	1025	2.4E-5	958	8.1E-6	955
C_4H_6	54	9.07	a	1,3-Butadiene	7.1E-4	1019	2.1E-4	963	6.1E-5	949
C_3H_4O	56	10.10	b	Acrolein	4.5E-4	1019	5.3E-4	958	6.9E-4	944
C_3H_6O	58	9.96	b	Propanal	7.3E-5	1025	7.8E-5	968	5.1E-5	949
C_5H_6	66	8.57	b	1,3-Cyclopentadiene	5.3E-4	1013	1.1E-5	968	1.8E-6	949
C_4H_4O	68	8.88	a	Furan	2.0E-4	1008	1.4E-4	958	fuel	
C_4H_6O	70	9.65	b	Methyl vinyl ketone	3.6E-4	1008	5.2E-4	958	-	-
C_4H_6O	70	9.73	b	2-Butenal	-	-	-	-	1.5E-5	949
C_4H_8O	72	9.52	b	2-Butanone	2.0E-5	1030	-	-	-	-
C_4H_8O	72	9.71	b	Isobutanal	-	-	2.2E-5	974	1.4E-5	949
C_6H_6	78	9.24	b	Benzene	3.9E-4	1041	2.1E-5	986	2.3E-6	955
C_5H_6O	82	8.38	a	2-Methylfuran	3.8E-4	1002	fuel		3.4E-6	944
C_7H_8	92	8.80	b	Toluene	3.7E-5	1030	3.8E-6	974	1.5E-6	955
C_6H_6O	94	8.49	b	Phenol	5.1E-4	1019	1.5E-5	968	4.5E-6	955
$C_5H_4O_2$	96	9.22	b	Furfural	-	-	2.4E-4	952	-	-
C_6H_8O	96	7.8	a	DMF	fuel		-	-	1.7E-6	949
C_8H_8	104	8.46	b	Styrene	1.1E-5	1036	1.4E-6	980	7.9E-7	955
C_8H_{10}	106	8.76	b	Ethylbenzene	1.0E-5	1036	1.8E-6	968	7.8E-7	949
$C_6H_6O_2$	110	NA	c	5-Methylfurfural	3.9E-4	985	-	-	-	-
C_9H_8	116	8.14	b	Indene	5.0E-6	1025	9.2E-7	991	8.4E-7	955
C_9H_{10}	118	8.54	b	Indane	6.3E-6	1030	1.3E-6	974	9.5E-7	955
$C_{10}H_8$	128	8.14	b	Naphthalene	7.1E-6	1036	9.5E-7	974	9.2E-7	949

For the conditions shown in Table 3, peak mole fractions for intermediate species detected in DMF, MF, and furan oxidation occur in the temperature ranges 985-1047 K, 952-986 K, and 944-955 K, respectively. The observed temperature interval is strongly fuel-dependent, *i.e.* 62 K for DMF, 34 K for MF, and 11 K for furan, consistent with the fuel conversion behavior described above, where the reaction zone for DMF oxidation spreads wider than those of MF and furan. The very thin reaction zone of furan oxidation makes it more difficult to identify the first products of its LMT oxidation.

Several categories of species in Table 3 merit further inspection. First, small species such as CH_4, C_2H_2, and C_2H_4 were detected with high mole fractions for all fuels, and their profiles reach maximum values at temperature higher than those at which the fuels are already completely consumed (compare Fig. 4). The formation of these species is strongly affected by the equivalence ratio for all three fuels; their mole fraction increase with increasing equivalence ratio (see Tables S4-S6).

The second class of species with peak mole fractions at high temperatures includes aromatic species such as C_6H_6 (benzene), C_7H_8 (toluene), C_8H_8 (styrene), C_8H_{10} (ethylbenzene), C_9H_8 (indene), C_9H_{10} (indane), and $C_{10}H_8$ (naphthalene). Bicyclic species including C_9H_8, C_9H_{10}, and $C_{10}H_8$ were detected with lower mole fractions of a few ppm, especially in the oxidation of MF and furan. These species are certainly formed by secondary reactions that are not the focus of the present work. Rather, we are interested in the formation of species at lower temperature, where LMT chemistry could be more predominant; these species will be discussed in the next sections.

3.2.2.1. Early-stage products

Species with *m/z*=110 (for DMF oxidation) and *m/z*=96 (for MF oxidation) exhibit maxima at the lowest temperatures. Moreover, these species are of higher mass than the respective fuels and were detected with high mole fractions ($\times 10^{-4}$). They could be key intermediates in the LMT oxidation of DMF and MF. The difference between *m/z*=110 and 96 corresponds exactly to that between the mass of DMF (*m/z*=96) and MF (*m/z*=82). If the same principle is applied to furan (*m/z*=68), the species at *m/z*=82 could be a key intermediate in the LMT oxidation of furan. However, as evident from Tables 3 and S6 (Supplemental Material 2), the species at *m/z*=82 was detected with very low mole fraction (a few ppm) even though its peak is found at the lowest temperature. Therefore, the main mechanism for the LMT oxidation of furan seems to be different. For furan, a low-temperature species at *m/z*=56 was detected with high mole fractions ($\times 10^{-4}$), which was evaluated as acrolein, and may be a product of OH-addition to the furan ring as it will be discussed later.

Hence, we now discuss first the formation of the species at *m/z*=110 and 96 in the oxidation of DMF and MF, respectively. Their mole fraction profiles are presented in Fig. 5. Based on a fuel-

destruction analysis, two species at *m/z*=110 could be expected for DMF oxidation, namely 5-methylfurfural ($C_6H_6O_2$) and 2-ethyl-5-methylfuran (MEF). Under the studied LMT conditions, the species was evaluated as 5-methylfurfural because its concentration is lower in the fuel-rich mixture than in stoichiometric and fuel-lean mixtures (see Fig. 5 and Table S4). This behavior indicates a more likely addition of oxygenated species – such as HO_2, CH_3O_2 – to fuel radicals to form higher-mass oxygenated species than addition of hydrocarbon species as *e.g.*, CH_3. The observed species at *m/z*=96 in MF oxidation, expected to be either furfural ($C_5H_4O_2$) or ethylfuran (EF), was evaluated as furfural for similar reasons. The LMT model predicts the formation trends of both species quite well and captures especially the effect of the equivalence ratio. Note that when the respective contributions of MEF and EF are taken into account, the simulated profiles in Fig. 5 will be affected only slightly in the lean case (~10%) and somewhat more significantly (up to ~70%) under fuel-rich conditions.

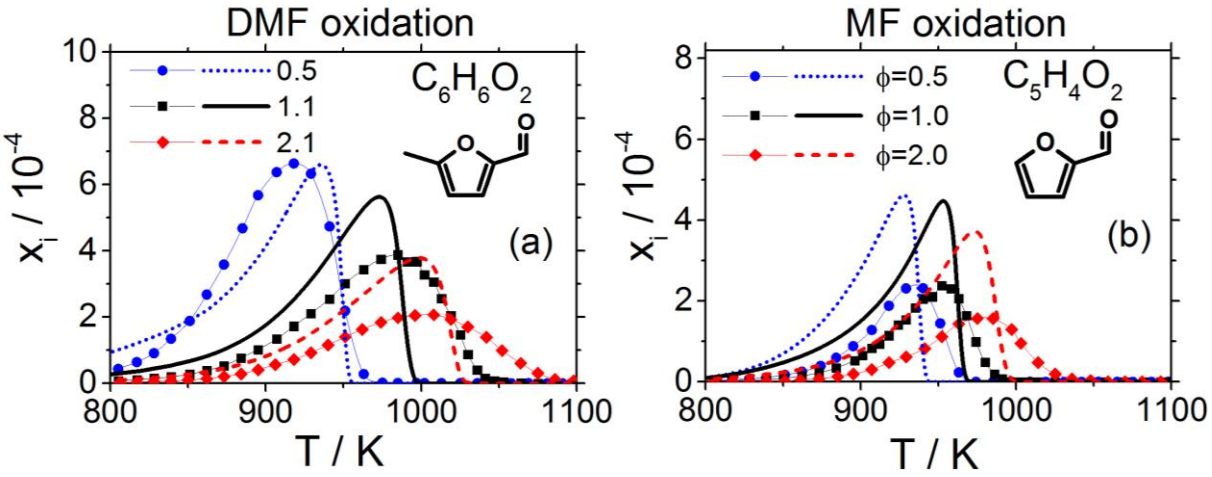

Figure 5. Low-temperature intermediates detected at *m/z*=110 and 96 in the oxidation of DMF (a) and MF (b), respectively. Species were evaluated as 5-methylfurfural ($C_6H_6O_2$) and furfural ($C_5H_4O_2$). *Symbols:* experiment at different equivalence ratios; *lines:* LMT model.

To better understand the early stages of the oxidation of DMF, MF, and furan in the present flow reactor, a ROP analysis of their consumption was performed with the LMT model at ϕ~1.0 (mixtures DMF1.0, MF1.0, F1.0), integrated over the region of 0-10% fuel conversion, corresponding to a temperature range of 900-950 K. The results of this analysis are shown in Fig. 6.

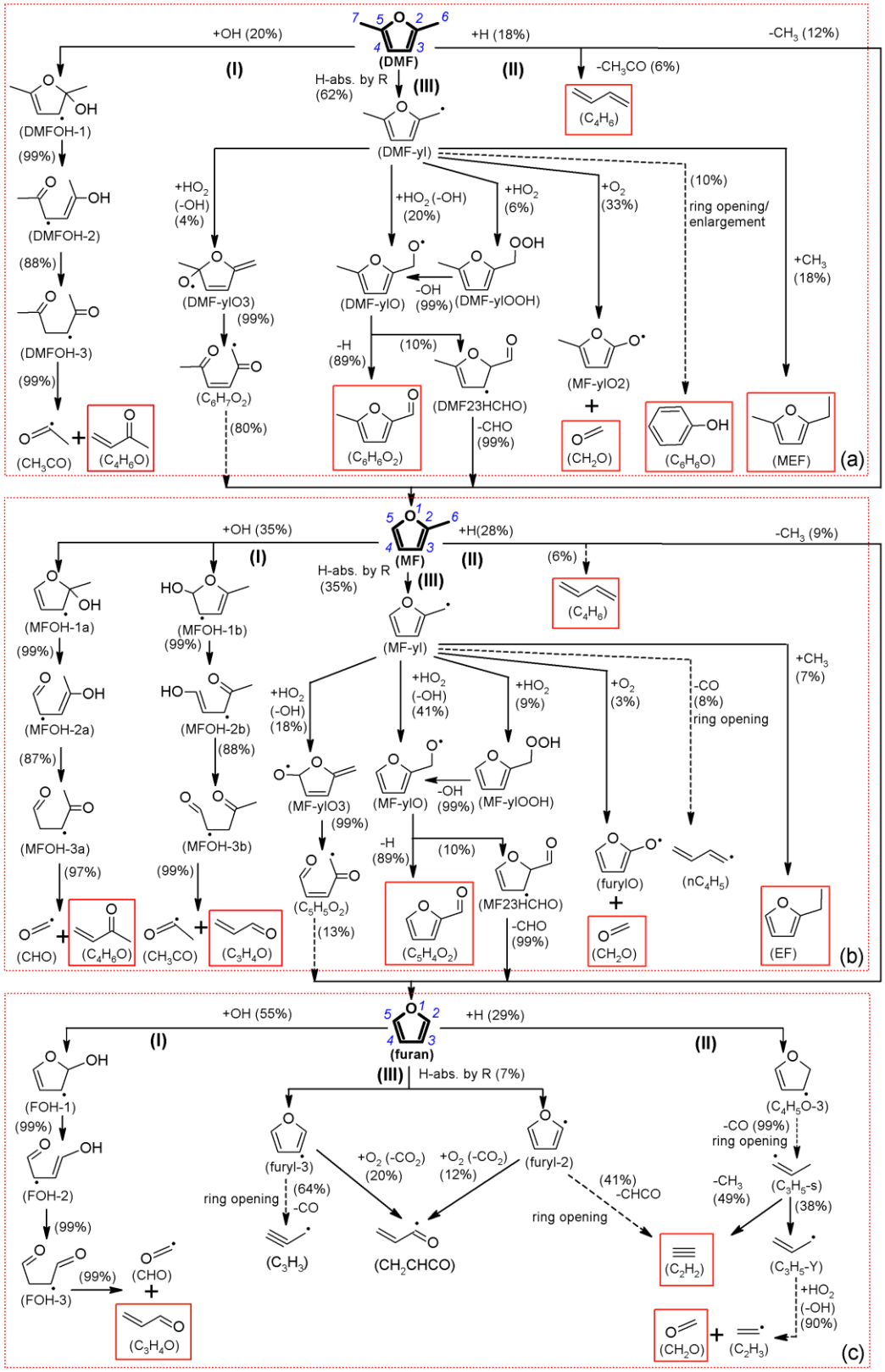

Figure 6. Reaction pathway (ROP) analysis for the consumption of DMF, MF, and furan at ϕ~1 (mixtures DMF1.0, MF1.0, F1.0) using the LMT model. Percentages given are relative rates of consumption of a species, integrated over the region of 0-10% fuel conversion that corresponds to a temperature range of 900-950 K. Primary stable intermediates are highlighted by solid boxes; they were also detected in the experiment. Dashed arrows represent the product(s) of a series of radical reactions within the current mechanism.

At the analyzed conditions, DMF is largely (62%) consumed by H-abstractions from the lateral methyl groups (channel **III**). H-abstraction reactions are still important for the consumption of MF (35%), but they make only a small contribution (7%) to furan consumption. This trend is in agreement with the difference in the number of lateral methyl group between the three fuels. Note that the BDE of the C–H bonds in the lateral methyl group (~85 kcal mol^{-1}) is much lower than that of the C–H bond in the ring (~119 kcal mol^{-1}) [21]. In the LMT range, OH-additions to the ring (channel **I**) become important, especially for furan, and contribute to the fuel consumption with 55% for furan, 35% for MF and 20% for DMF. This higher importance of OH-addition for furan *versus* MF and DMF results from the slow H-abstractions from furan. Fuel consumption through H-addition reactions (channel **II**) is not as significant, but still relevant with 29% for furan, 28% for MF, and 18% for DMF. Note that all primary stable species resulting from these important pathways (identified by boxes in Fig. 6) were detected in the experiment with relatively high mole fractions (Tables 3, S4-S6). It is also worth noting that most of the reactions of the fuel radicals DMF-yl and MF-yl that were theoretically investigated in the present study appear in the ROP analyses and demonstrate the importance of such systematic computations.

Indeed, it is seen by following the pathways in Fig. 6 that the resonance-stabilized DMF-yl and MF-yl radicals react with HO_2 to form OH and DMF-ylO or MF-ylO (Note that reactions with CH_3O_2 showed only minor contributions and have thus been omitted in Fig. 6 for simplicity). DMF-ylO and MF-ylO in turn decompose to H + $C_6H_6O_2$ or H + $C_5H_4O_2$. These furfural species were found to reach their maximum mole fractions at the lowest temperatures, as described above, and largely consumed by H-abstractions from the lateral carbonyl group due to the weakness of C─H bonds in the (BDE ~90 kcal mol^{-1}) (not shown in Fig 6). Since these reaction sequences produce two reactive species, namely OH and H, they are very important in controlling the reactivity and their detailed and accurate description is therefore highly valuable. This explains why the present LMT model can predict the fuel conversion, primary species such as furfural species ($C_6H_6O_2$ and $C_5H_4O_2$), and species produced by comparative pathways such as phenol (C_6H_6O) much better than the published previous HT version [22] (see Fig. S17 in Supplemental Material 2).

For a better overview of the fuel reactions over temperature ranges and equivalence ratios used in the present flow reactor, we have performed ROP analyses for DMF, MF, and furan at higher fuel conversions (*i.e.* higher temperatures) than those in Fig. 6 as well as for the fuel-lean/-rich mixtures. The results for all these conditions indicate the same reactions to be involved in the fuel consumption, however, their respective importance is different. While the consumption of all three fuels was considered for 0-10% conversion in Fig. 6, increasing the fuel conversion to 90% enhances the importance of H-addition to the double bonds by approximately 60%. Also, that of the ring opening of the fuel radicals increases by a factor up to three, whereas that of reactions of fuel radicals with O_2 is reduced fourfold. When keeping the same fuel conversion but decreasing or increasing the equivalence ratio, the importance of reactions involving oxygenated species such as O_2, OH and HO_2 is slightly enhanced or reduced, respectively, while an opposite behavior is noted for reactions involving non-oxygenated species such as H and CH_3. Exemplarily, when the equivalence ratio decreases from 1 to 0.5, the contribution of the OH-addition reactions to the consumption of DMF and MF increases by ~30%. Similarly, the consumption reactions are sensitively influenced by the CH_3 radical with a decrease of the recombination of DMF-yl and MF-yl with CH_3 by 40% when decreasing the equivalence ratio from 1.0 to 0.5.

3.2.2.2. Formaldehyde and other key species

Reactions of the fuel radicals DMF-yl and MF-yl with O_2 contribute to their consumption with 33% and 3%, respectively (Fig. 6), leading to the formation of formaldehyde. Furthermore, as mentioned earlier, the mole fraction of CH_2O increases very early in DMF oxidation. The measured CH_2O profile for DMF oxidation is shown in Fig. 7 (for mixture DMF1.0) together with species involved in the DMF-yl reactions including $C_6H_6O_2$ and C_6H_6O (phenol); also, C_2H_6 is included that is known to be formed mainly from CH_3 self-recombination to indicate the presence of CH_3.

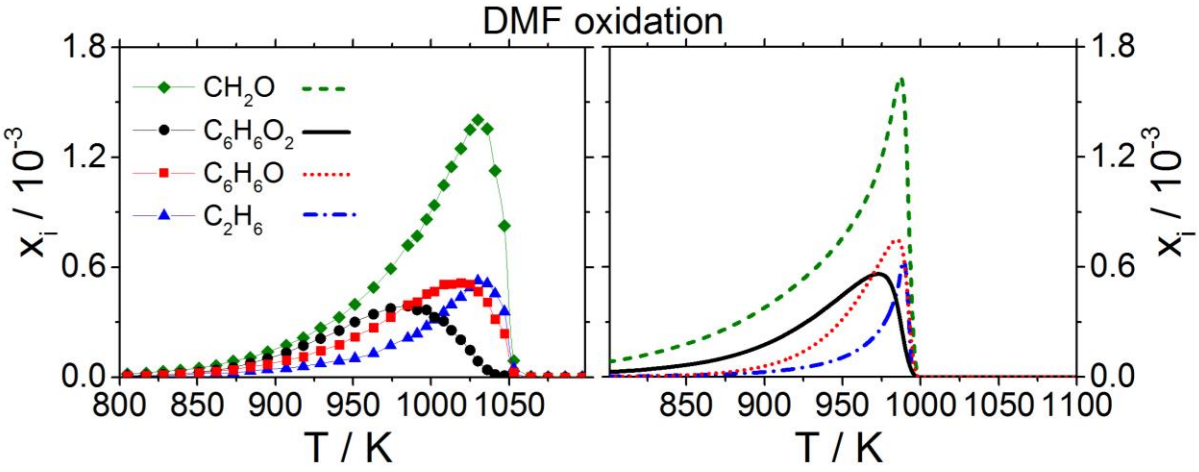

Figure 7. Mole fraction profiles of CH_2O (formaldehyde) and of selected primary products of fuel radical reactions in DMF oxidation (DMF1.0 mixture): $C_6H_6O_2$ (5-methyl-2-furfural) and C_6H_6O (phenol); also included is the profile of C_2H_6 (ethane) as a typical CH_3 recombination product. *Left panel:* experiment, *right panel:* LMT model.

Relative trends between species profiles from the experiments and simulations are in quite good agreement, with simulated peak positions shifted to lower temperature, however. Especially $C_6H_6O_2$ and CH_2O mole fractions increase quite early as an indication of LMT reactions. Indeed the ROP analysis at low (~10%) DMF conversion shows about 50% of CH_2O to be formed by the reaction DMF-yl + O_2 ⇆ CH_2O + MF-ylO2. CH_2O reaches its maximum only at relative high temperature, however, and at a similar peak location as C_2H_6, indicating the presence of CH_3 that might thus contribute to the formation of CH_2O at high temperatures. From a ROP analysis with increasing temperature, CH_3O (+M) ⇆ CH_2O +H (+M) is seen to gain substantial importance above 980 K over the DMF-yl + O_2 ⇆ CH_2O + MF-ylO2 reaction that is dominant in the low-temperature regime. The inclusion of the DMF-yl + O_2 reaction leads to improved predictions of CH_2O yields with the LMT model in comparison to the model of Somers *et al.* [17,27,28], especially in the fuel-lean case (see Fig. S18 in Supplemental Material 2). It is important to note that, according to sensitivity analyses, the reaction DMF-yl + O_2 is also found to considerably enhance the conversion of DMF, especially under fuel-lean conditions (compare Fig. S18) as mentioned earlier. Phenol that is known as an important species resulting from a ring opening/ring enlargement reaction sequence from the DMF-yl radical [21], was detected with lower mole fraction than CH_2O and a maximum at lower temperature than CH_2O and C_2H_6 (see Fig. 7). This trend is also well predicted by the model.

Regarding the consumption of MF, the contribution of MF-yl + O_2 is smaller than in the analogous case for DMF (compare Figs. 6a, 6b). Nevertheless, as shown in Fig. 8, the mole fraction profile of CH_2O increases already at low temperatures. At low fuel conversion, the ROP analysis indicates that the reactions MF-yl + O_2 contribute only in part to the formation of CH_2O (Fig. 6b). Another source for CH_2O is the reaction of MF-yl with CH_3O_2 which forms CH_3O and MF-ylO, both in turn can decompose to form CH_2O. Similarly to the case of DMF, the CH_2O profile peaks at relatively higher temperature than primary species from the fuel radical (MF-yl) such as $C_5H_4O_2$ (furfural) and C_4H_4 (vinylacetylene), see Fig. 8a and Table 3 (for MF1.0) for the same reasons as discussed above for DMF. At low temperatures, the contribution of ring opening *via* the formation of *n*-C_4H_5 radical to the production of C_4H_4 is less important than reactions of this radical with oxygenated species; therefore C_4H_4 was detected with low concentration although it exhibits its maximum at low temperature (Table 3, Fig. 8a). Both the experimental and simulated results are in reasonable agreement regarding relative trends. The simulated profiles, especially that of CH_2O, are noted to decrease faster, pointing towards a possible influence of the aforementioned self-sustaining combustion in the high-temperature range.

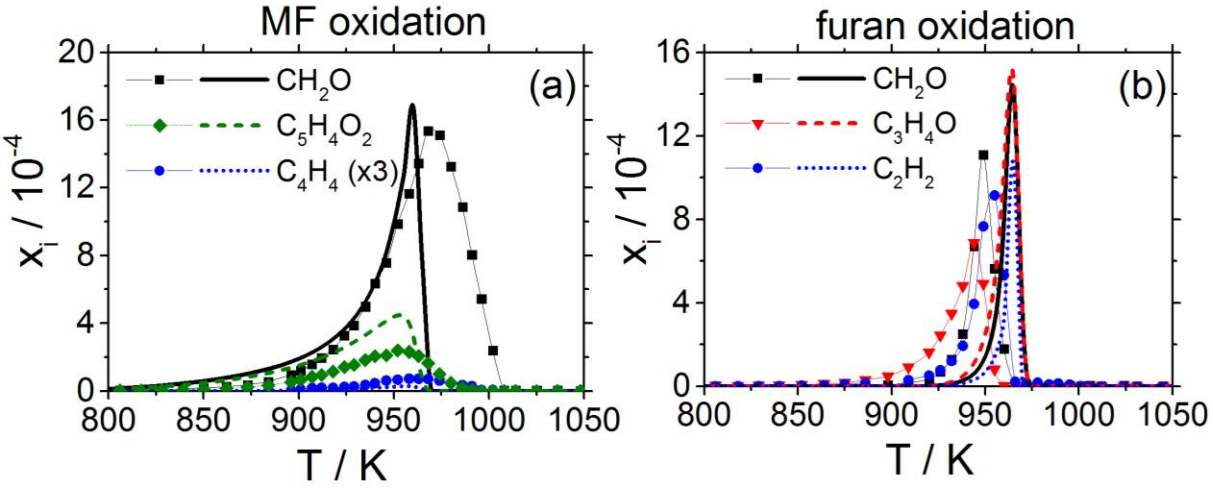

Figure 8. (a) MF oxidation at ϕ~1 (MF1.0 mixture): mole fraction profiles of CH_2O and selected primary products of fuel radical reactions including $C_5H_4O_2$ (furfural) and C_4H_4 (vinylacetylene); for C_4H_4, results from experiment and simulation were multiplied by a factor of 3 to facilitate comparison. (b) Furan oxidation at ϕ~1 (F1.0 mixture): mole fraction profiles of C_3H_4O (acrolein), CH_2O, and C_2H_2. *Symbols:* experiment, *lines:* LMT model.

Figure 8b provides the mole fraction profile of the lowest-temperature intermediate for furan oxidation, acrolein, together with CH_2O and C_2H_2. Significant differences were found in comparison to the DMF and MF experiments under similar conditions. Firstly, the present experiments did not identify high concentrations of primary intermediates resulting directly from the fuel radicals, *i.e.* furyl-2 and furyl-3. The reason is that H-abstractions from furan are very slow, resulting in low concentrations of the furyl-2 and furyl-3 radicals. Only a species at *m/z*= 82, evaluated as MF, was detected at very low mole fractions (2.9×10^{-6} - 4.1×10^{-6}, see Tables 3 and S6) that could be produced from the recombination of furyl-2 with CH_3. Second, the reaction zone in furan oxidation is very thin, and it is difficult to distinguish the locations of the maximum mole fraction in Fig. 8b. It seems that the experimental profile of C_3H_4O increases already at lower temperatures than those of C_2H_2 and CH_2O, and the LMT model predicts this trend correctly. According to the ROP analysis, C_3H_4O is mainly produced via several steps starting from OH-addition at the C2 or C5 positions of the furan ring (channel **I** in Fig. 6c). This reaction sequence is the main consumption path of furan at LMT conditions, suggesting that OH-addition to the ring could be the most important process under these conditions. This behavior is, thirdly, again different in comparison to that of DMF and MF for which the reactions of fuel radicals (DMF-yl, MF-yl) with small oxygenated species to produce furfurals seem more important. Fourth, the profile of CH_2O (Fig. 8b) at low fuel conversion behaves differently from those for DMF and MF oxidation: While CH_2O can be produced from reactions of the fuel radical (DMF-yl and MF-yl) in DMF and MF oxidation, respectively, the ROP analysis for furan oxidation indicates that CH_2O is not a result of the reactions of the fuel radicals (furyl-2 and furyl-3), but mainly produced from the reaction of HO_2 with allyl (C_3H_5-Y) radical that is mainly a product of H-addition to the furan ring (channel **II** in Fig. 6c).

The reactions of channel **I** in Fig. 6, namely OH-addition to the C2 or C5 positions of the ring, lead to the formation of acrolein (C_3H_4O) for furan oxidation as mentioned above (Fig. 6c) and produce mainly methyl vinyl ketone (C_4H_6O) in DMF oxidation (Fig. 6a). Due to the asymmetric structure of MF, OH-addition to MF leads to the formation of both C_3H_4O and C_4H_6O (Fig. 6b). These species were detected with quite high mole fractions in the experiment (Table 3). Comparing the temperatures

for their occurrence determined in the experiments, these products, namely C_4H_6O in DMF oxidation as well as C_4H_6O and C_3H_4O in MF oxidation, exhibit their maxima at higher temperatures than 5-methylfurfural and furfural, respectively (Table 3). The mole fraction profiles of C_4H_6O and C_3H_4O are given in Fig. 9 for ϕ~1 (DMF1.0, MF1.0, F1.0 conditions) for the three fuels. The model over-predicts the peak mole fractions of these species by factors of 1.5-2, close to the experimental uncertainty, while differences are noted in the shapes of the profiles especially for DMF and furan. Interestingly, the prediction for DMF oxidation suggests a maximum at lower temperatures while the opposite trend is seen for furan oxidation, indicating that different mechanisms could contribute to this behavior. Part of the discrepancies could be influenced by the adopted high-pressure limiting rate coefficients for the OH-addition reactions that were available in the literature [28,61], and thus suggest a more detailed treatment of the possibly complex pressure dependence of this reaction class.

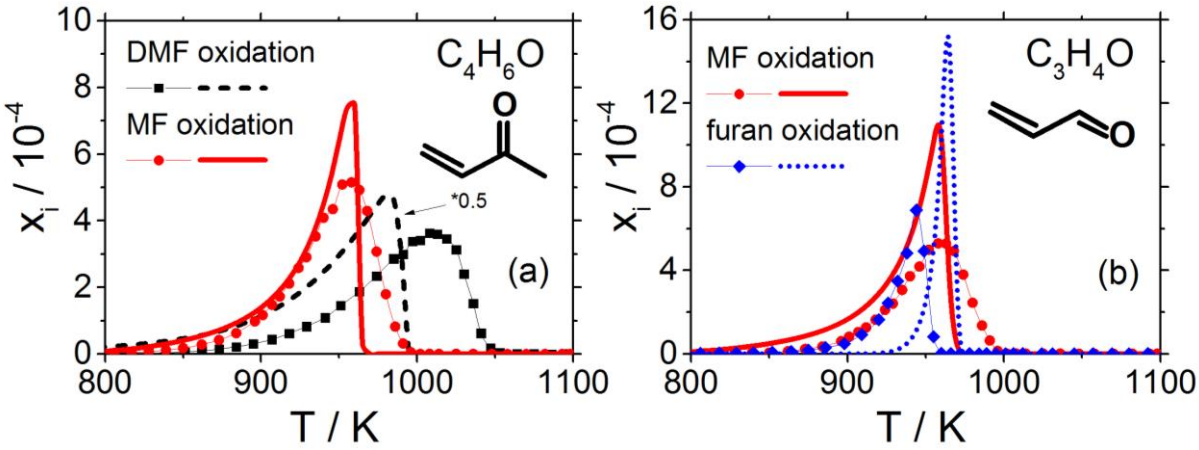

Figure 9. Mole fraction profiles of C_4H_6O (methyl vinyl ketone) and C_3H_4O (acrolein), *i.e.* two main products of OH-addition to DMF, MF, and furan at ϕ~1 (DMF1.0, MF1.0, F1.0 mixtures). *Symbols:* experiment; *lines:* LMT model.

The sequential occurrence of OH- and H-addition reactions is addressed in Fig. 10 for DMF and MF. The mole fraction of acrolein as the product of OH-addition to the furan ring was seen to increase already at lower temperatures than those of CH_2O and C_2H_2 as the products of H-addition (see Fig. 8b). This sequence is also experimentally observed for MF oxidation as demonstrated in Fig. 10b, where C_4H_6O, a selected product of OH-addition to MF, rises earlier than that of C_4H_6 (1,3-butadiene),

a selected species of H-addition to MF. This trend is well predicted by the model, and it seems logical because OH-addition is dominant at LMT conditions, whereas H-addition is important at higher temperatures. The same trend is also predicted for DMF oxidation by the model, with a similar low-temperature increase for both species seen in the experimental data in this case (Fig. 10a). This may be in contrast with the results for DMF in a JSR at 10 bar of Somers *et al.* [17] which showed the mole fraction of C_4H_6 to increase significantly slower than that of C_4H_6O at these conditions.

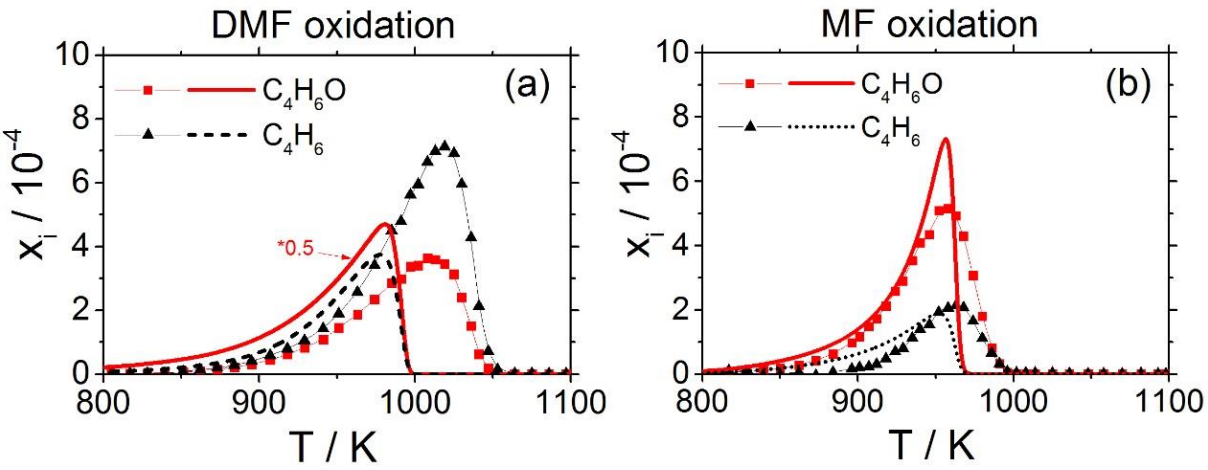

Figure 10. Comparison of the sequence of OH- and H-addition reactions to the furan ring. The mole fractions of C_4H_6O (methyl vinyl ketone), a selected product of OH-addition to the ring, and C_4H_6 (1,3-butadiene), a selected product of H-addition to the ring are shown for DMF and MF oxidation at ϕ~1 (DMF1.0, MF1.0 mixtures). *Symbols:* experiment, *lines:* LMT model.

3.2.2.3. Influence of equivalence ratio on key intermediates

Figure 11 addresses the influence of equivalence ratio by presenting maximum mole fractions of selected primary fuel-specific intermediates in the oxidation of DMF, MF, and furan at lean (ϕ~0.5), near-stoichiometric (ϕ~1), and rich (ϕ~2) conditions. In each case, key intermediates were chosen as products from HO_2, O_2, and OH-addition as well as reaction pathways involving H-atoms and CH_3 radicals. For DMF (Fig. 11a), both experiment and simulation show a strong effect of equivalence ratio on the formation of intermediates. As might be expected, mole fractions of CH_2O, C_4H_6O, and $C_6H_6O_2$ – resulting from channels that involve oxygenated reactants – decrease with increasing equivalence ratio, whereas those of C_4H_6, C_5H_6O, and C_6H_6O – to a major extent products of pathways

such as addition of H or CH_3 as well as ring opening/enlargement reactions – are seen to increase. In the case of MF (Fig. 11b), a largely similar pattern is seen where again mole fractions of C_4H_6O and $C_5H_4O_2$ as products of MF-yl reactions with HO_2 and OH-addition pathways decrease not unexpectedly with increasing equivalence ratio, whereas both C_4H_6 and C_4H_4O (results of H-addition reactions) increase with increasing equivalence ratio. For CH_2O and C_3H_4O, somewhat different trends are seen in experiment and simulation. Especially in the case of furan (Fig. 11c), the effect of equivalence ratio on CH_2O in particular seems not significant. The lack of lateral methyl groups limits the role of abstraction reactions and this might be the reason for this small dependence of intermediate species yields on the equivalence ratio. The somewhat contrasting behavior between DMF and furan could result from the importance of the DMF-yl + O_2 for CH_2O formation in DMF oxidation *versus* the simultaneous dependence of the CH_2O formation on H-addition and subsequent reaction with HO_2 in the case of furan.

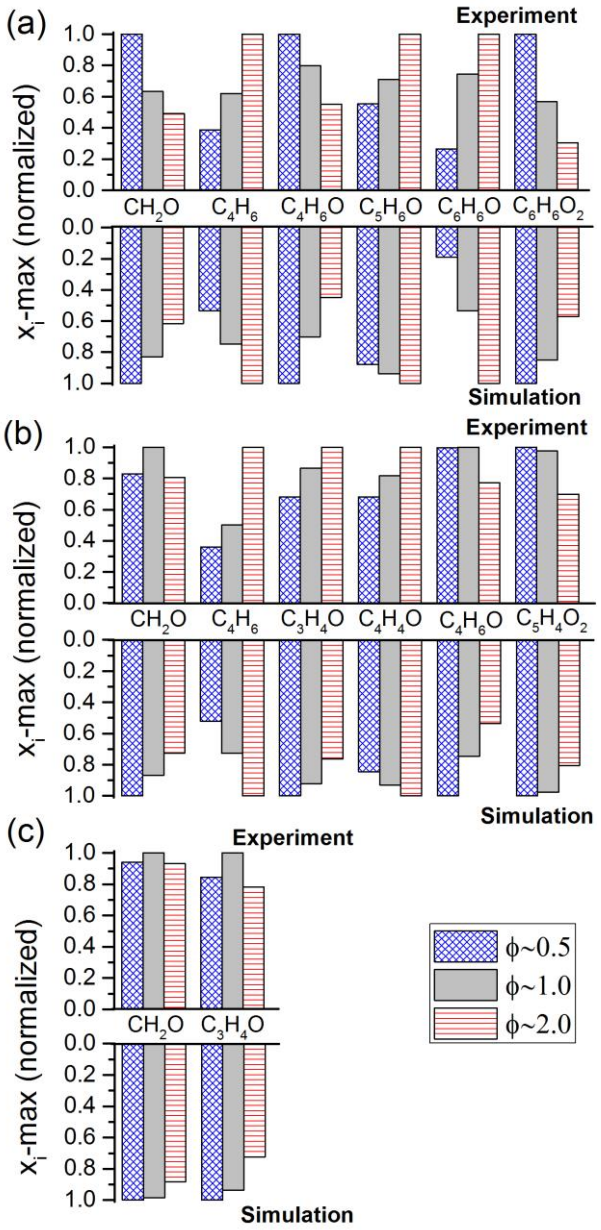

Figure 11. Effects of equivalence ratio on the maximum mole fractions of selected fuel-specific intermediates in the oxidation of DMF (a), MF (b), and furan (c). *In each figure, top:* experiment, *bottom:* LMT model. For clarity, normalization by the highest value is performed, and mole fraction scales have been inverted for the simulations.

3.2.3. Comparison of the formation of potential pollutants

Since the clean combustion performance of advanced biofuels is a key aspect of their use, we have analyzed and will compare the formation of potential pollutants by the three furanic fuels. For the first time, this comparison can be systematically performed between DMF, MF, and furan under the present

near-identical LMT conditions. It can also be extended to analyze such trends between the flow reactor and flame configurations, addressing different pressure, temperature, and transport regimes.

3.2.3.1. Comparison between DMF, MF, and furan at LMT conditions

Figure 12 presents the experimental and simulated maximum mole fractions of selected undesirable and hazardous species formed during the oxidation of DMF, MF, and furan for near-stoichiometric conditions (*i.e.* DMF1.0, MF1.0, and F1.0), together with the structure of the respective main expected isomer and its pollutant potential based on [62,63]. These pollutants include firstly selected highly toxic/carcinogenic species, such as formaldehyde (CH_2O), ketene (C_2H_2O), acrolein (C_3H_4O), methyl vinyl ketone (C_4H_6O), phenol (C_6H_6O), and furfural ($C_5H_4O_2$), and secondly important soot precursors such as acetylene (C_2H_2), propene (C_3H_6), 1,3-butadiene (C_4H_6), 1,3-cyclopentadiene (C_5H_6), benzene (C_6H_6), and naphthalene ($C_{10}H_8$). Note that some of these soot precursors are also carcinogenic. The hazard identification of 5-methylfurfural ($C_6H_6O_2$) seems not yet clear, but because of its specificity in DMF oxidation, this species is also included in this comparison.

As a very important result it must be noted that several highly toxic species were experimentally detected and consistently predicted by the LMT model for these conditions. In general, maximum mole fractions of small species such as C_2H_2 and CH_2O are quite similar for the three fuels, whereas the formation of larger hazardous species is very different, with their nature depending strongly on the fuel structure. Under near-identical conditions, the oxidation of DMF and MF produces much higher amounts of C_4H_6O than the oxidation of furan. Furthermore, DMF oxidation produces substantially more C_2H_2O, C_6H_6O, $C_6H_6O_2$, and soot precursors. However, MF oxidation results in much larger mole fractions of $C_5H_4O_2$, and a concern of the furan oxidation is the production of higher amounts of C_3H_4O. However, the formation of C_3H_4O is also not negligible for DMF and MF oxidation. The high ability of the furanic fuels to form C_3H_4O and C_4H_6O is related to the important influence of the OH-addition to the furan ring under LMT conditions (compare Fig. 6) that leads directly to the formation of these species. Based on sensitivity analyses, the formation of these highly toxic species produced in DMF and MF oxidation was found to be strongly related to the reactions

DMF + O_2, DMF-yl + O_2, DMF-yl + HO_2 (for DMF) as well as MF + O_2, MF-yl + O_2, DMF-yl + HO_2 (for MF), which have been theoretically calculated in the present work.

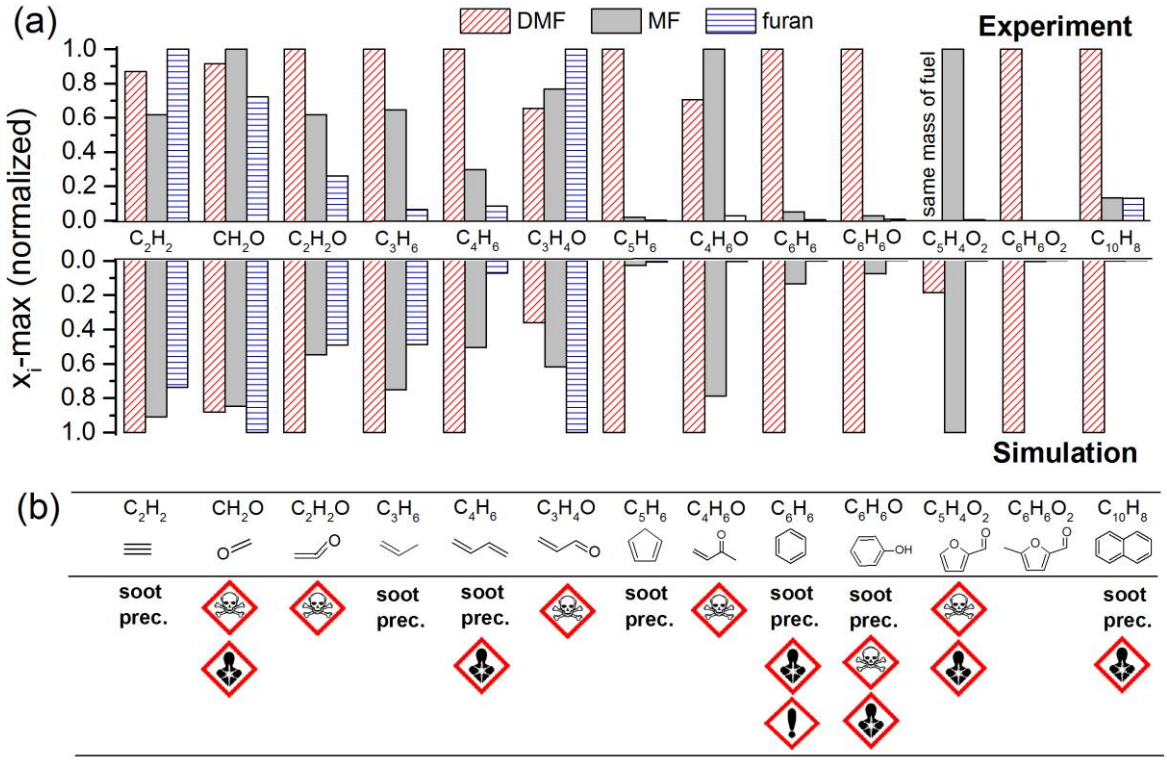

Figure 12. (a) Maximum mole fractions of selected undesirable and hazardous compounds for DMF, MF, and furan oxidation. *Top:* experiments at ϕ~1 (DMF1.0, MF1.0, F1.0 mixtures), *bottom:* LMT model predictions. For clarity, normalization by the highest value is performed, and mole fraction scales have been inverted for the simulations. (b) Structure of the respective main expected isomer and its pollutant potential based on [62,63]. Hazard pictograms are based on the Globally Harmonized System of Classification and Labelling of Chemicals (GHS) system. *Soot prec.:* soot precursor.

Both experiment and model indicate that $C_5H_4O_2$ is formed in much higher mole fractions during MF oxidation (Fig. 12) than in DMF and furan oxidation, because, as described above, furfural can be produced directly by a dominant path of fuel radical (MF-yl) consumption at LMT conditions (Fig. 6b). $C_6H_6O_2$ is a fuel-specific intermediate of DMF oxidation at LMT conditions (Fig. 6a), therefore its mole fraction is much higher for DMF than for MF and furan (Fig. 12). This induces also a higher amount of C_2H_2O in DMF oxidation, because ketene is formed, under the present conditions, largely from a pathway starting from 5-methylfurfural through a succession of H-abstractions/CO

elimination/ring opening/β-scission reactions leading to the formation of propargyl radical (C_3H_3) which in turn reacts with O_2 to form ketene by the reaction $C_3H_3 + O_2 \leftrightarrows C_2H_2O + CHO$.

DMF has a higher ability to form phenol and soot precursors compared to less substituted furans. Similar trends have been also observed in previous premixed flames [21,22], and in part also in non-premixed flame studies [64] where especially MF may also form additional soot precursors in high quantities such as benzene. For the flow reactor conditions investigated here, the main routes leading to the formation of phenol and soot precursors from DMF seem quite similar to those under flame conditions [21,22]. This ability results from the ring enlargement of a radical yielded from the ring opening of the resonance-stabilized DMF-yl radical. As demonstrated from theoretical calculations and detailed in the study of Sirjean *et al.* [24], due to the availability of the second lateral methyl group, the DMF-yl radical can favorably react by ring enlargement through several steps to give cyclohexa-2,4-diene-1-one which subsequently forms phenol. In Fig. 6a this route is globally called "ring opening/enlargement", and the pressure-dependent rate coefficients of reactions involved in this succession were included in the present model. This ring enlargement reaction is not possible for MF and furan because of an absence of the second lateral methyl group, for which fuel radicals decompose into CO and smaller hydrocarbons. Subsequent reactions of phenol contribute to the formation of other soot precursors such as benzene and 1,3-cyclopentadiene, which contribute to naphthalene ($C_{10}H_8$) formation via cyclopentadienyl (C_5H_5) self-recombination.

3.2.3.2. Comparison between flow reactor and flame

To expand the discussed conditions, it may be interesting to compare the present flow reactor data with results obtained previously in a premixed flame configuration [19-21] regarding overall oxidation behavior and pollutant emissions of the furanic fuels. Note that these studies have been performed using the same analytical technique (EI-MBMS).

Before discussing differences in species distribution between flow reactor and flame experiments, it is important to note that – regarding the overall oxidation behavior – the contribution of H-abstractions to the fuel consumption in both configurations increases in the sequence

DMF>MF>furan, as a result of the difference in the number of lateral methyl groups. Under flame conditions, H-addition to the furan ring contributed dominantly to the fuel consumption [19-21], whereas OH-addition to the furan ring becomes important for the flow reactor conditions. Furthermore, in flames, fuel radicals are consumed mainly by thermal decomposition, whereas reactions of fuel radicals with oxygenated species including O_2, HO_2, and CH_3O_2 play important roles under flow reactor conditions.

Concerning species formation, we have compared their selectivity for both configurations at an identical, sufficient extent of 80% fuel conversion for near-stoichiometric conditions. This level of fuel conversion corresponds to temperatures of ~950-1000 K in the flow reactor and ~1200-1400 K in flames. The selectivity was experimentally determined as the ratio of the mole fraction of a species versus the sum of the mole fractions of all detected intermediate species (*i.e.* not including the main species fuel, O_2, Ar, H_2, CO, CO_2, and H_2O in this sum). The comparison is shown in Fig. 13. Note that species with $m/z<30$ (such as CH_4, C_2H_2, C_2H_4), which have high total selectivity, are not shown for clarity. In the flame, reactions of the fuels lead dominantly to the formation of these small species with a total selectivity of ~50-60%, compared to ~40-50% in the flow reactor. Therefore species at masses above 30 are generally observed to show lower selectivity in the flame (Fig. 13b) than in the flow reactor (Fig. 13a). It is very important to note that several oxygenated species, highlighted with bold front, such as ketene (C_2H_2O), methyl vinyl ketone (C_4H_6O), phenol (C_6H_6O), furfural ($C_5H_4O_2$), and 5-methylfurfural ($C_6H_6O_2$), occur with high selectivity in the flow reactor, whereas they are not represented in the flame configuration. Moreover, two other oxygenated toxic species, formaldehyde (CH_2O) and acrolein (C_3H_4O), are formed with high amounts in both configurations and exhibit slightly higher selectivity in the flow reactor than in the flame. In summary, the selectivity towards oxygenated species – some of them highly toxic – demonstrates their importance as primary products of the LMT oxidation of the furanic fuels in the flow reactor. While the present results, obtained for an unprecedentedly large parameter set for these fuels studied systematically by combining experiment, theory and simulation, should raise some caution that such hazardous compounds may also result from practical combustion systems, especially when using LMT strategies, further analyses

are necessary to systematically assess effects of mixing, pressure, and dilution such as in exhaust gas recirculation.

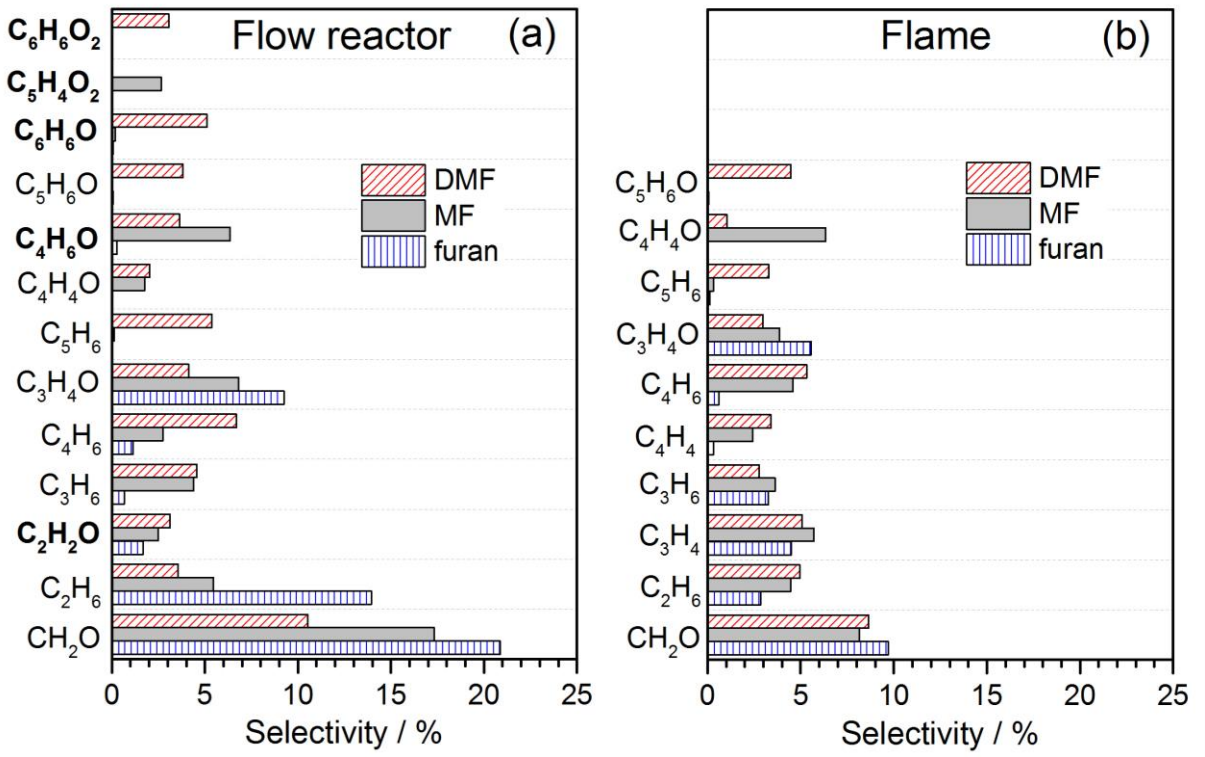

Figure 13. Comparison of the selectivity of intermediate species, at ϕ~1 and ~80% fuel conversion, between the present flow reactor (a) and previously studied flames [19-21] (b). Selectivity was experimentally determined as the ratio of the mole fraction of a species (at ~80% fuel conversion) versus the sum of the mole fractions of all intermediate species (*i.e.* not including the main species fuel, O_2, Ar, H_2, CO, CO_2, H_2O). Species with *m/z*<30 (CH_4, C_2H_2, C_2H_4) that exhibit a high total selectivity of 40-50% in the flow reactor and 50-60% in the flame, are not shown for clarity. Presented species have a selectivity ≥2% for at least one fuel. Species highlighted with **bold** front occur only in selectivity calculations with flow reactor data.

4. Summary and perspectives

The present study provides the first dataset of quantitative species profiles for the three furanic fuels DMF, MF, and furan under near-identical LMT conditions in a flow reactor at atmospheric pressure. These new experimental results from an EI-MBMS analysis report more than 35 species profiles at each condition. By itself, this dataset is a valuable contribution to compare the reactivity and product distribution, and it served also to motivate the development of the present kinetic model with the aim to describe the LMT oxidation chemistry of these fuels in more accurate detail. The present LMT

model distinguishes itself from other literature models by including, for the first time, detailed reaction subsets for HO_2- and O_2-addition to the two most important resonance-stabilized fuel radicals, 2-furylmethyl (MF-yl) and 5-methyl-2-furanylmethyl (DMF-yl). The kinetic data of these reaction subsets were computed using high-level theoretical calculations. Moreover, H-abstractions from MF and DMF by O_2, identified as a sensitive reaction class for the LMT oxidation of these fuels, were also newly computed using accurate theoretical methods. As a result, a single model for the three furanic fuels was presented encompassing both, LMT and HT reaction conditions. The fuel conversion behavior and the formation of fuel-specific intermediate species were analyzed, and important differences between three fuels have been highlighted. Several highly toxic oxygenated species such as formaldehyde, acrolein, methyl vinyl ketone, furfural, and phenol, were detected with high concentrations and were identified as primary products of the furanic fuel oxidation under LMT conditions. While the absolute reactivity of the three fuels investigated might change at technical combustion conditions, the potential formation of highly toxic oxygenated species in the LMT regime could be always expected because these species are produced from most of the main competitive consumption paths of the furanic fuels. Indeed, recent engine studies [65] have demonstrated that toxic species including 1,3-butadiene, formaldehyde, benzene, acetaldehyde, and furan can be formed in the combustion of DMF in a single cylinder direct-injection spark-ignition engine.

Although the present work improves the understanding of the oxidation behavior of the furanic fuels, it is clear that further developments are needed in the simulation method, the kinetic model, as well as the experiment. Some suggested avenues for further research could include a more extensive experimental investigation especially at more highly diluted LMT conditions to suppress self-sustaining combustion phenomena completely. Especially at higher pressures, detailed speciation data at identical LMT conditions for all three fuels are still very scarce and would merit further investigation. Moreover, it may be valuable to study the LMT oxidation chemistry of crucial primary species individually, such as for the sub-systems of 5-methylfurural, furfural, 2-ethyl-5-methylfuran, and 2-ethylfuran, to assist further model developments.

Concerning the kinetic model, the use of high-pressure-limiting rate coefficients for OH-addition to the fuel ring – a reaction class of importance for the LMT consumption of furanic fuels – involves some uncertainties in model predictions for the corresponding products versus those from competing pathways. High-level theoretical calculations are thus recommended to further investigate the pressure dependence of this reaction class for the three furanic fuels. Furthermore, during DMF and MF simulations, the system reactivity was found to be sensitive to the recombination of the resonance-stabilized DMF-yl and MF-yl radicals with CH_3, respectively. Again this would be a valuable subject for further theoretical calculations. Moreover, some differences remain between experiment and model in the case of furan conversion. As mentioned earlier, two sets of kinetic data for H-abstractions from the furan ring by HO_2 and CH_3O_2 were thus tested. The first set is taken from the RMG database [43], whereas the second was thought to lead to potential improvements by using the result of the present CBS-QB3 calculation for the H-abstraction rate coefficient from the C3 position of furan by HO_2 as an approximation for H-abstractions by HO_2 and CH_3O_2 from all carbon sites of furan. Although the H-abstraction reactions with HO_2 and CH_3O_2 do not significantly contribute directly to furan consumption, these two kinetic data sets resulted in very different simulated reactivity as presented in Fig. S20 (Supplemental Material 2). In spite of the more global treatment, the first set represents the reactivity quite well, whereas furan consumption is under-predicted with the second, theoretically slightly more involved kinetic approach. Interestingly, a similar influence of the two different kinetic sets is not seen for the JSR conditions of Thorton *et al.* [31] (see Fig. S7). The prediction of the furan reactivity with the model of Somers *et al.* [28] is even less satisfactory for the present conditions (Fig. S20).

To improve the prediction quality in this case, further reactions have been considered. Note that all reaction classes adopted for DMF and MF have also been applied to furan. While some of them are very important in controlling the system reactivity of DMF and MF oxidation, as *e.g.*, reactions of fuel radicals with HO_2, they seem of no importance to the furan conversion. Additional possible reaction classes for furan oxidation, such as direct O_2-addition and HO_2-addition to furan were tentatively included with estimated kinetic data [41-43], but they were also found to be unimportant

for fuel conversion and thus finally omitted in the present LMT model, mainly to avoid complexity and additional uncertainty. Furthermore, as a last test in the present work, we computed, using the theoretical methods above, the Diels-Alder reaction between two furan molecules to form a bicyclic species ($C_8H_8O_2$, see Fig. S21 in Supplemental Material 2), that can subsequently react with O_2 to supply reactive radicals to the system. These reactions were found to have much lower barriers than the direct bimolecular initiation reactions of furan with O_2. However, all these additions to the mechanism did not increase the simulated reactivity for furan. Therefore the prediction of the reactivity during the oxidation of furan under low- to medium-temperature conditions remains an interesting but potentially difficult subject that will need further experimental and theoretical investigations.

Acknowledgements

Luc-Sy Tran is grateful to the Alexander von Humboldt (AvH) Foundation for a research fellowship. Zhandong Wang was supported by a fellowship granted by the China Scholarship Council for performing part of his thesis work in Bielefeld. The authors also wish to thank Casimir Togbé, Orléans, France, for his contribution to some of the experiments during his research period in Bielefeld that was supported by the AvH Foundation, as well as Olivier Herbinet, Nancy, France, for his contribution to some of the simulation work. Finally, we would like to acknowledge valuable contributions of Friederike Herrmann, DLR Stuttgart, Germany, to the construction of the reactor and to some experiments while she performed her thesis in Bielefeld.

Authorship statement

Zhandong Wang performed the experiments during his stay in Bielefeld. Hans-Heinrich Carstensen designed and carried out the theoretical work. Christian Hemken assisted with the formulation of the non-isothermal reactor model. Luc-Sy Tran developed the kinetic model in interaction with Frédérique Battin-Leclerc, and he and Katharina Kohse-Höinghaus directed the collaborative work and wrote the paper.

References

[1] A.J. Janssen, F.W. Kremer, J.H. Baron, M. Muether, S. Pischinger, J. Klankermayer, Tailor-made fuels from biomass for homogeneous low-temperature diesel combustion, Energy Fuels 25 (2011) 4734–4744.

[2] T.W. Rudolph, J.J. Thomas, NOx, NMHC and CO emissions from biomass derived gasoline extenders, Biomass 16 (1988) 33–49.

[3] M. Thewes, M. Muether, S. Pischinger, M. Budde, A. Brunn, A. Sehr, P. Adomeit, J. Klankermayer, Analysis of the impact of 2-methylfuran on mixture formation and combustion in a direct-injection spark-ignition engine, Energy Fuels 25 (2011) 5549–5561.

[4] C. Wang, H. Xu, R. Daniel, A. Ghafourian, J.M. Herreros, S. Shuai, X. Ma, Combustion characteristics and emissions of 2-methylfuran compared to 2,5-dimethylfuran, gasoline and ethanol in a DISI engine, Fuel 103 (2013) 200–211.

[5] Q. Zhang, G. Chen, Z. Zheng, H. Liu, J. Xu, M. Yao, Combustion and emissions of 2,5-dimethylfuran addition on a diesel engine with low temperature combustion, Fuel 103 (2013) 730–735.

[6] W. Leitner, J. Klankermayer, S. Pischinger, H. Pitsch, K. Kohse-Höinghaus, Advanced biofuels and beyond: Chemistry solutions for propulsion and production, Angew. Chem. Int. Ed., DOI: 10.1002/anie.201607257.

[7] M.R. Grochowski, W. Yang, A. Sen, Mechanistic study of a one-step catalytic conversion of fructose to 2,5-dimethyltetrahydrofuran, Chem.-Eur. J. 18 (2012) 12363–12371.

[8] Y. Román-Leshkov, C.J. Barrett, Z.Y. Liu, J.A. Dumesic, Production of dimethylfuran for liquid fuels from biomass-derived carbohydrates, Nature 447 (2007) 982–986.

[9] J.-P. Lange, E. van der Heide, J. van Buijtenen, R. Price, Furfural - A promising platform for lignocellulosic biofuels, ChemSusChem 5 (2012) 150–166.

[10] G. Chen, Y. Shen, Q. Zhang, M. Yao, Z. Zheng, H. Liu, Experimental study on combustion and emission characteristics of a diesel engine fueled with 2,5-dimethylfuran-diesel, n-butanol-diesel and gasoline-diesel blends, Energy 54 (2013), 333–342.

[11] H. Liu, J. Xu, Z. Zheng, S. Li, M. Yao, Effects of fuel properties on combustion and emissions under both conventional and low temperature combustion mode fueling 2,5-dimethylfuran/diesel blends, Energy 62 (2013) 215–223.

[12] S. Jouzdani, M.A. Eldeeb, L. Zhang, B. Akih-Kumgeh, High-temperature study of 2-methyl furan and 2-methyl tetrahydrofuran combustion, Int. J. Chem. Kinet. 48 (2016) 491–503.

[13] L.-S. Tran, B. Sirjean, P.-A. Glaude, R. Fournet, F. Battin-Leclerc, Progress in detailed kinetic modeling of the combustion of oxygenated components of biofuels, Energy 43 (2012) 4–18.

[14] Y. Uygun, S. Ishihara, H. Olivier, A high pressure ignition delay time study of 2-methylfuran and tetrahydrofuran in shock tubes, Combust. Flame 161 (2014) 2519–2530.

[15] G. Vanhove, Y. Yu, M.A. Boumehdi, O. Frottier, O. Herbinet, P.-A. Glaude, F. Battin-Leclerc, Experimental study of tetrahydrofuran oxidation and ignition in low- temperature conditions, Energy Fuels 29 (2015) 6118–6125.

[16] R. Tripathi, C. Lee , R.X. Fernandes, H. Olivier, H.J. Curran, S.M. Sarathy, H. Pitsch, Ignition characteristics of 2-methyltetrahydrofuran: An experimental and kinetic study, Proc. Combust. Inst. 36 (2017) 587–595.

[17] K.P. Somers, J.M. Simmie, F. Gillespie, C. Conroy, G. Black, W.K. Metcalfe, F. Battin-Leclerc, P. Dirrenberger, O. Herbinet, P.-A. Glaude, P. Dagaut, C. Togbé, K. Yasunaga, R.X. Fernandes, C. Lee, R. Tripathi, H.J. Curran, A comprehensive experimental and detailed chemical kinetic modelling study of 2,5-dimethylfuran pyrolysis and oxidation, Combust. Flame 160 (2013) 2291–2318.

[18] Z. Tian, T. Yuan, R. Fournet, P.-A. Glaude, B. Sirjean, F. Battin-Leclerc, K. Zhang, F. Qi, An experimental and kinetic investigation of premixed furan/oxygen/argon flames, Combust. Flame 158 (2011) 756–773.

[19] D. Liu, C. Togbé, L.-S. Tran, D. Felsmann, P. Oßwald, P. Nau, J. Koppmann, A. Lackner, P.-A. Glaude, B. Sirjean, R. Fournet, F. Battin-Leclerc, K. Kohse-Höinghaus, Combustion chemistry and flame structure of furan group biofuels using molecular-beam mass spectrometry and gas chromatography - Part I: Furan, Combust. Flame 161 (2014) 748–765.

[20] L.-S. Tran, C. Togbé, D. Liu, D. Felsmann, P. Oßwald, P.-A. Glaude, R. Fournet, B. Sirjean, F. Battin-Leclerc, K. Kohse-Höinghaus, Combustion chemistry and flame structure of furan group biofuels using molecular-beam mass spectrometry and gas chromatography - Part II: 2-Methylfuran, Combust. Flame 161 (2014) 766–779.

[21] C. Togbé, L.-S. Tran, D. Liu, D. Felsmann, P. Oßwald, P.-A. Glaude, B. Sirjean, R. Fournet, F. Battin-Leclerc, K. Kohse-Höinghaus, Combustion chemistry and flame structure of furan group biofuels using molecular-beam mass spectrometry and gas chromatography - Part III: 2,5-Dimethylfuran, Combust. Flame 161 (2014) 780–797.

[22] L.-S. Tran, B. Sirjean, P.-A. Glaude, K. Kohse-Höinghaus, F. Battin-Leclerc, Influence of substituted furans on the formation of Polycyclic Aromatic Hydrocarbons in flames, Proc. Combust. Inst. 35 (2015) 1735–1743.

[23] M. Conturso, M. Sirignano A. D'Anna, Effect of furanic biofuels on particles formation in premixed ethylene–air flames: An experimental study, Fuel 175 (2016) 137–145.

[24] B. Sirjean, R. Fournet, P.-A. Glaude, F. Battin-Leclerc, W. Wang, M.A. Oehlschlaeger, Shock tube and chemical kinetic modeling study of the oxidation of 2,5-dimethylfuran, J. Phys. Chem. A 117 (2013) 1371–1392.

[25] N. Xu, C. Tang, X. Meng, X. Fan, Z. Tian, Z. Huang, Experimental and kinetic study on the ignition delay times of 2,5-dimethylfuran and the comparison to 2-methylfuran and furan, Energy Fuels 29 (2015) 5372–5381.

[26] M.A. Eldeeb, B. Akih-Kumgeh, Reactivity trends in furan and alkyl furan combustion, Energy Fuels 28 (2014) 6618–6626.

[27] K.P. Somers, J.M. Simmie, F. Gillespie, U. Burke, J. Connolly, W.K. Metcalfe, F. Battin-Leclerc, P. Dirrenberger, O. Herbinet, P.-A. Glaude, H.J. Curran, A high temperature and

atmospheric pressure experimental and detailed chemical kinetic modelling study of 2-methyl furan oxidation, Proc. Combust. Inst. 34 (2013) 225–232.

[28] K.P. Somers, J.M. Simmie, W.K. Metcalfe, H.J. Curran, The pyrolysis of 2-methylfuran: a quantum chemical, statistical rate theory and kinetic modelling study, Phys. Chem. Chem. Phys. 16 (2014) 5349–5367.

[29] N. Xu, J. Gong, Z. Huang. Review on the production methods and fundamental combustion characteristics of furan derivatives, Renew. Sustain. Energy Rev. 54 (2016) 1189–1211.

[30] N. Xu, Y. Wu, C. Tang, P. Zhang, X. He, Z. Wang, Z. Huang, Experimental study of 2,5-dimethylfuran and 2-methylfuran in a rapid compression machine: Comparison of the ignition delay times and reactivity at low to intermediate temperature, Combust. Flame 168 (2016) 216–227.

[31] M.M. Thorton, P.C. Malte, A.L. Crittenden, Oxidation of furan and furfural in a well-stirred reactor, Symp. (Int.) Combust. 21 (1988) 979–989.

[32] K. Alexandrino, Á. Millera, R. Bilbao, M.U. Alzueta, Interaction between 2,5-dimethylfuran and nitric oxide: Experimental and modeling study, Energy Fuels 28 (2014) 4193–4198.

[33] K. Alexandrino, Á. Millera, R. Bilbao, M.U. Alzueta, Novel aspects in the pyrolysis and oxidation of 2,5-dimethylfuran, Proc. Combust. Inst. 35 (2015) 1717–1725.

[34] K. Alexandrino, Á. Millera, R. Bilbao, M.U. Alzueta, 2-Methylfuran oxidation in the absence and presence of NO, Flow Turb. Combust. 96 (2016) 343–362.

[35] A.C. Davis, S.M. Sarathy, Computational study of the combustion and atmospheric decomposition of 2-methylfuran, J. Phys. Chem. A 117 (2013) 7670–7685.

[36] Z. Wang, X. Zhang, L. Xing, L. Zhang, F. Herrmann, K. Moshammer, F. Qi, K. Kohse-Höinghaus, Experimental and kinetic modeling study of the low- and intermediate-temperature oxidation of dimethyl ether, Combust. Flame 162 (2015) 1113–1125.

[37] F. Herrmann, P. Oßwald, K. Kohse-Höinghaus, Mass spectrometric investigation of the low-temperature dimethyl ether oxidation in an atmospheric pressure laminar flow reactor, Proc. Combust. Inst. 34 (2013) 771–778.

[38] F. Herrmann, B. Jochim, P. Oßwald, L. Cai, H. Pitsch, K. Kohse-Höinghaus, Experimental and numerical low-temperature oxidation study of ethanol and dimethyl ether, Combust. Flame 161 (2014) 384–397.

[39] G. da Silva, J.W. Bozzelli, Kinetic modeling of the benzyl + HO_2 reaction, Proc. Combust. Inst. 32 (2009) 287–294.

[40] Y. Murakami, T. Oguchi, K. Hashimoto, Y. Nosaka, Theoretical study of the benzyl + O_2 reaction: Kinetics, mechanism, and product branching ratios, J. Phys. Chem. A 111 (2007) 13200–13208.

[41] G.M. Côme, V. Warth, P.A. Glaude, R. Fournet, F. Battin-Leclerc, G. Scacchi, Computer-aided design of gas-phase oxidation mechanisms - Application to the modeling of *n*-heptane and iso-octane oxidation, Symp. (Int.) Combust. 26 (1996) 755-762.

[42] B. Husson, M. Ferrari, O. Herbinet, S.S. Ahmed, P.-A. Glaude, F. Battin-Leclerc, New experimental evidence and modeling study of the ethylbenzene oxidation, Proc. Combust. Inst. 34 (2013) 325-333.

[43] C.W. Gao, J.W. Allen, W.H. Green, R.H. West, Reaction Mechanism Generator: Automatic construction of chemical kinetic mechanisms, Comput. Phys. Commun. 203 (2016) 212–225.

[44] C. Muller, V. Michel, G. Scacchi, G.M. Côme, THERGAS: a computer program for the evaluation of thermochemical data of molecules and free radicals in the gas phase, J. Chim. Phys. PCB 92 (1995) 1154–1178.

[45] S.W. Benson, Thermochemical kinetics: Methods for the estimation of thermochemical data and rate parameters, John Wiley & Sons, New York, 1976.

[46] H. Wang, M. Frenklach, Transport properties of Polycyclic Aromatic Hydrocarbons for flame modeling, Combust. Flame 96 (1994) 163–170.

[47] J.A. Montgomery, Jr., M.J. Frisch, J.W. Ochterski, G.A. Petersson, A complete basis set model chemistry. VI. Use of density functional geometries and frequencies, J. Chem. Phys. 110 (1999) 2822–2827.

[48] M.J. Frisch, G.W. Trucks, H.B. Schlegel, G.E. Scuseria, M.A. Robb, J.R. Cheeseman, G. Scalmani, V. Barone, B. Mennucci, G.A. Petersson, H. Nakatsuji, M. Caricato, X. Li, H.P. Hratchian, A.F. Izmaylov, J. Bloino, G. Zheng, J.L. Sonnenberg, M. Hada, M. Ehara, K. Toyota, R. Fukuda, J. Hasegawa, M. Ishida, T. Nakajima, Y. Honda, O. Kitao, H. Nakai, T. Vreven, J.A. Montgomery, Jr., J.E. Peralta, F. Ogliaro, M. Bearpark, J.J. Heyd, E. Brothers, K.N. Kudin, V.N. Staroverov, R. Kobayashi, J. Normand, K. Raghavachari, A. Rendell, J.C. Burant, S.S. Iyengar, J. Tomasi, M. Cossi, N. Rega, J.M. Millam, M. Klene, J.E. Knox, J.B. Cross, V. Bakken, C. Adamo, J. Jaramillo, R. Gomperts, R.E. Stratmann, O. Yazyev, A.J. Austin, R. Cammi, C. Pomelli, J.W. Ochterski, R.L. Martin, K. Morokuma, V.G. Zakrzewski, G.A. Voth, P. Salvador, J.J. Dannenberg, S. Dapprich, A.D. Daniels, Ö. Farkas, J.B. Foresman, J.V. Ortiz, J. Cioslowski, D.J. Fox, Gaussian 09, Revision D.01, Gaussian, Inc., Wallingford CT, 2009.

[49] L.A. Curtiss, K. Raghavachari, P.C. Redfern, J.A. Pople, Assessment of Gaussian-2 and density functional theories for the computation of enthalpies of formation, J. Chem. Phys. 106 (1997) 1063–1079.

[50] A.L.L. East, L. Radom, Ab initio statistical thermodynamical models for the computation of third-law entropies, J. Chem. Phys. 106 (1997) 6655–6674.

[51] G.A. Petersson, D.K. Malick, W.G. Wilson, J.W. Ochterski, J.A. Montgomery, Jr., M.J. Frisch, Calibration and comparison of the Gaussian-2, complete basis set, and density functional methods for computational thermochemistry, J. Chem. Phys. 109 (1998) 10570–10580.

[52] M.K. Sabbe, M. Saeys, M.-F. Reyniers, G.B. Marin, V. Van Speybroeck, M. Waroquier, Group additive values for the gas phase standard enthalpy of formation of hydrocarbons and hydrocarbon radicals, J. Chem. Phys. A 109 (2005) 7466–7480.

[53] J.A. Manion, R.E. Huie, R.D. Levin, D.R. Burgess Jr., V.L. Orkin, W. Tsang, W.S. McGivern, J.W. Hudgens, V.D. Knyazev, D.B. Atkinson, E. Chai, A.M. Tereza, C.-Y. Lin, T.C. Allison, W.G. Mallard, F. Westley, J.T. Herron, R.F. Hampson, D.H. Frizzell, NIST Chemical Kinetics Database, NIST Standard Reference Database 17, Version 7.0 (Web Version), Release 1.6.8,

Data version 2015.12, National Institute of Standards and Technology, Gaithersburg, Maryland, 20899-8320. Available at: < http://kinetics.nist.gov>.

[54] A.M. Dean, Predictions of pressure and temperature effects upon radical addition and recombination reactions, J. Phys. Chem. 89 (1985) 4600–4608.

[55] A.Y. Chang, J.W. Bozzelli, A.M. Dean, Kinetic analysis of complex chemical activation and unimolecular dissociation reactions using QRRK theory and the modified strong collision approximation, Z.Phys. Chem. 214 (2000) 1533–1568.

[56] H.-H. Carstensen, A.M. Dean, A quantitative kinetic analysis of CO elimination from phenoxy radicals, Int. J. Chem. Kinet. 44 (2012) 75–89.

[57] LOGEsoft. Available at: <http://loge.se/Products/LOGE_Products.html>.

[58] Python. Available at: <https://www.python.org/>

[59] J.M. Simmie, W.K. Metcalfe, Ab initio study of the decomposition of 2,5-dimethylfuran, J. Phys. Chem. A 115 (2011) 8877–8888.

[60] H. Wang, X. You, A.V. Joshi, S.G. Davis, A. Laskin, F. Egolfopoulos, C.K. Law, USC Mech Version II. High-temperature combustion reaction model of H_2/CO/C_1-C_4 compounds, May 2007. Available at: < http://ignis.usc.edu/USC_Mech_II.htm>.

[61] S.H. Mousavipour, S. Ramazani, Z. Shahkolahi, Multichannel RRKM-TST and direct-dynamics VTST study of the reaction of hydroxyl radical with furan, J. Phys. Chem. A 113 (2009) 2838–2846.

[62] Sigma-Aldrich Company. Available at: <http://www.sigmaaldrich.com>.

[63] Toxicology data network-U.S. National Library of Medicine. Available at: <https://chem.nlm.nih.gov/chemidplus/>.

[64] M. Sirignano, M. Conturso, A. D'Anna, Effect of furans on particle formation in diffusion flames: An experimental and modeling study, Proc. Combust. Inst. 35 (2015) 525–532.

[65] R. Daniel, L. Wei, H. Xu, C. Wang, M.L. Wyszynski, S. Shuai, Speciation of hydrocarbon and carbonyl emissions of 2,5-dimethylfuran combustion in a DISI engine, Energy Fuels 26 (2012) 6661–6668.

Figure Captions

Figure 1. Rate coefficients of H-abstractions from MF and DMF by O_2 calculated in the present work and used in the present LMT model, compared with those estimated and used in the Somers *et al.* model [28], and with those estimated by EXGAS software [41] used in our previously published HT model [22].

Figure 2. Pathways of the bimolecular reactions of the resonance-stabilized 2-furylmethyl (MF-yl) and 5-methyl-2-furanylmethyl (DMF-yl) radicals with the HO_2 radical. Thick arrows denote major channels that were included in the pressure dependence analysis. Below the arrows, rate constants calculated at 940 K are provided.

Figure 3. Pathways of the bimolecular reaction of MF-yl and DMF-yl with O_2. Thick arrows denote major channels that were included in the pressure dependence analysis. Below the arrows, rate constants calculated at 940 K are provided.

Figure 4. Fuel mole fractions as a function of reactor temperature. Symbols: experiment; lines: LMT model.

Figure 5. Low-temperature intermediates detected at *m/z*=110 and 96 in the oxidation of DMF (a) and MF (b), respectively. Species were evaluated as 5-methylfurfural ($C_6H_6O_2$) and furfural ($C_5H_4O_2$). *Symbols:* experiment at different equivalence ratios; *lines:* LMT model.

Figure 6. Reaction pathway (ROP) analysis for the consumption of DMF, MF, and furan at ϕ~1 (mixtures DMF1.0, MF1.0, F1.0) using the LMT model. Percentages given are relative rates of consumption of a species, integrated over the region of 0-10% fuel conversion that corresponds to a temperature range of 900-950 K. Primary stable intermediates are highlighted by solid boxes; they were also detected in the experiment. Dashed arrows represent the product(s) of a series of radical reactions within the current mechanism.

Figure 7. Mole fraction profiles of CH_2O (formaldehyde) and of selected primary products of fuel radical reactions in DMF oxidation (DMF1.0 mixture): $C_6H_6O_2$ (5-methyl-2-furfural) and C_6H_6O

(phenol); also included is the profile of C_2H_6 (ethane) as a typical CH_3 recombination product. *Left panel:* experiment, *right panel:* LMT model.

Figure 8. (a) MF oxidation at ϕ~1 (MF1.0 mixture): mole fraction profiles of CH_2O and selected primary products of fuel radical reactions including $C_5H_4O_2$ (furfural) and C_4H_4 (vinylacetylene); for C_4H_4, results from experiment and simulation were multiplied by a factor of 3 to facilitate comparison. (b) Furan oxidation at ϕ~1 (F1.0 mixture): mole fraction profiles of C_3H_4O (acrolein), CH_2O, and C_2H_2. *Symbols:* experiment, *lines:* LMT model.

Figure 9. Mole fraction profiles of C_4H_6O (methyl vinyl ketone) and C_3H_4O (acrolein), *i.e.* two main products of OH-addition to DMF, MF, and furan at ϕ~1 (DMF1.0, MF1.0, F1.0 mixtures). *Symbols:* experiment; *lines:* LMT model.

Figure 10. Comparison of the sequence of OH- and H-addition reactions to the furan ring. The mole fractions of C_4H_6O (methyl vinyl ketone), a selected product of OH-addition to the ring, and C_4H_6 (1,3-butadiene), a selected product of H-addition to the ring are shown for DMF and MF oxidation at ϕ~1 (DMF1.0, MF1.0 mixtures). *Symbols:* experiment, *lines:* LMT model.

Figure 11. Effects of equivalence ratio on the maximum mole fractions of selected fuel-specific intermediates in the oxidation of DMF (a), MF (b), and furan (c). *In each figure, top:* experiment, *bottom:* LMT model. For clarity, normalization by the highest value is performed, and mole fraction scales have been inverted for the simulations.

Figure 12. (a) Maximum mole fractions of selected undesirable and hazardous compounds for DMF, MF, and furan oxidation. *Top:* experiments at ϕ~1 (DMF1.0, MF1.0, F1.0 mixtures), *bottom:* LMT model predictions. For clarity, normalization by the highest value is performed, and mole fraction scales have been inverted for the simulations. (b) Structure of the respective main expected isomer and its pollutant potential based on [62,63]. Hazard pictograms are based on the Globally Harmonized System of Classification and Labelling of Chemicals (GHS). *Soot prec.:* soot precursor.

Figure 13. Comparison of the selectivity of intermediate species, at ϕ~1 and ~80% fuel conversion, between the present flow reactor (a) and previously studied flames [19-21] (b). Selectivity was experimentally determined as the ratio of the mole fraction of a species (at ~80% fuel conversion) versus the sum of the mole fractions of all intermediate species (*i.e.* not including the main species fuel, O_2, Ar, H_2, CO, CO_2, H_2O). Species lighter with m/z<30 (CH_4, C_2H_2, C_2H_4) that exhibit a high total selectivity of 40-50% in the flow reactor and 50-60% in the flame, are not shown for clarity. Presented species have a selectivity ≥2% for at least one fuel. Species highlighted with **bold** front occur only in selectivity calculations with flow reactor data.

List of Supplemental Material

1/ Experimental data of the present flow-reactor study (excel file)

2/ Additional data for simulation method, model development, and experiments (pdf file)

3/ Mechanism (CHEMKIN file)

Thermodynamic properties (CHEMKIN file)

Transport properties (CHEMKIN file)

4/ New rate coefficients from theoretical computations in the present study (txt file)